POLITECNICO
MILANO 1863

DIPARTIMENTO DI ELETTRONICA
INFORMAZIONE E BIOINGEGNERIA

Measurements of Laser Beam Using Knife Edge Technique

Presented by: Mohamed Moustafa Rashad,
Matricola: 883668
Under supervision of Professor: Cesare Svelto

Acknowledgments

First of all, I would like to thank my thesis advisor professor Cesare Svelto of the Department of Electronics, Information, and Bioengineering in the Polytechnic university of Milano, whom his office door was always open whenever I had a question about my research or writing. Not only did he consistently allow this study to see the light, but he also guided me in the right direction whenever I needed it.

Finally, I must express my deep gratefulness to my family and friends for providing me with unfailing support and continuous encouragement throughout my years of study and through the process of researching and writing this thesis. This accomplishment would not have been possible without them. Thank you.

Author

Mohamed Rashad

Contents

Chapter 1: Introduction to Lasers

LASER stands for Light Amplification by Stimulated Emission of Radiation. The lasers are devices that produce light of a specific color (wavelength) that depends on the parameters of design. Their output can be as small as a pencil-thin beam that conserves its concentration as it travels through long distances. Lasers play a key role in a lot of technologies. This chapter will understand the quality parameters of the laser and get an overview of the methods used to measure their quality parameters.

1.1 Laser Beam Profile Quality Parameters

Lasers have proven their importance in many technologies of modern life. The further the quality of the laser beam improves the more accurate will the devices perform. There are many parameters of a laser beam such as:-

-Beam Quality

For the Gaussian beams, this is one of the most important parameters of concern. It is the illumination pattern. It is independent of the wavelength. Its quantitative factor is called M^2. It indicates how close the beam is to the fundamental mode TEM_{00}, Gaussian beam. It determines how small the beam spot size can be as well as beam divergence. Figure 1.1 shows the different transverse modes that can be present in a laser beam.

- Beam Width

There are over five definitions for the beamwidth. The definition of particular interest for this study is the $1/e^2$. It defines the beam width as the distance between two points at which the measured power is 0.135 of the maximum value. For a Gaussian beam, the relationship between the FWHM and the $1/e^2$ is $2w=1.699*FWHM$, where $2w$ is the full width of the beam at $1/e^2$ of peak intensity.

-Beam Profile

The 2-dimensional plot of the intensity profile at a given location on the beam flight path. There many different ideal beam profiles. The profile mainly depends on the purpose. The most two common ones are the Gaussian beam profile and the flat top profiles, which are shown in figures 1.2 and 1.3 respectively. The beam profile importance is that it impacts the energy density, its concentration, and the collimation of the light. Moreover, the propagation of the beam through space is greatly influenced by the beam profile. However, due to imperfections in the devices, some deformations may occur to the output beam. Figures 1.4-a, b, and c show several deformed laser beam profiles showing the varieties that can exist.

-Beam Divergence

In electro-optics, the beam divergence is defined as the angular measure of the spreading of the beam as it travels away from the source. It is particularly relevant in the far-field. The output light of a laser is confined in the shape of a narrow cone; however, at long distances, it slowly spreads. The divergence is the angular measure of the increase in the diameter at distance from the optical device. There will be further explanations on beam divergence in this study and how to measure it quantitatively.

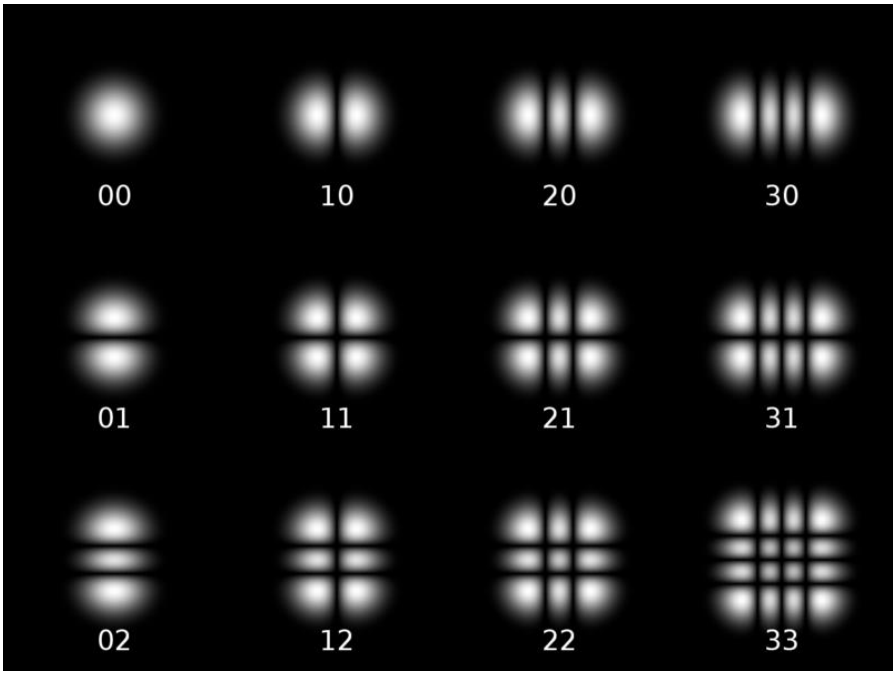

Figure 1.1 Different profiles of the transverse electromagnetic modes. The one of concern is theTEM_{00}, which is the Gaussian fundamental beam

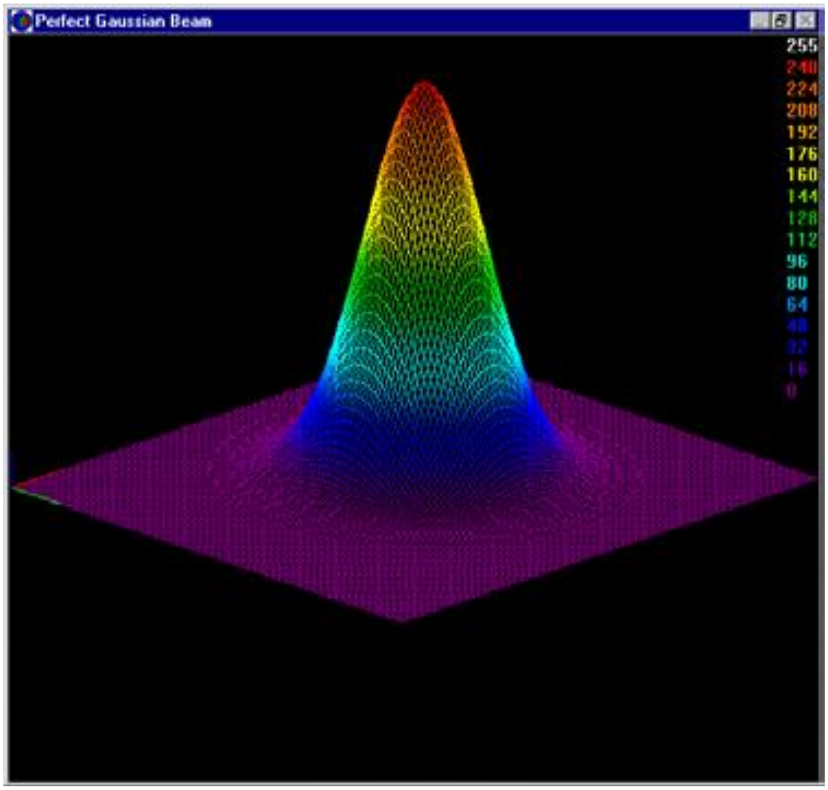

Figure 1.2 Profile of the ideal Gaussian beam, TEM_{00}. The intensity is at zenith at the center and decreases as the point of measurement fades away from the center

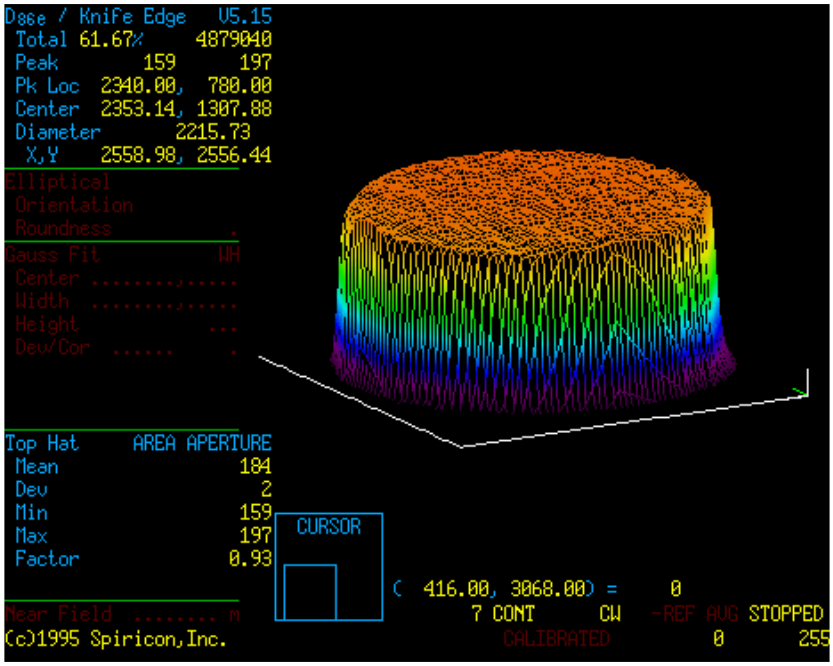

Figure 1.3 Flat-top laser beam profile for uniform laser illumination, in which the power level is constant across the propagation plan and decreases steeply on the edges

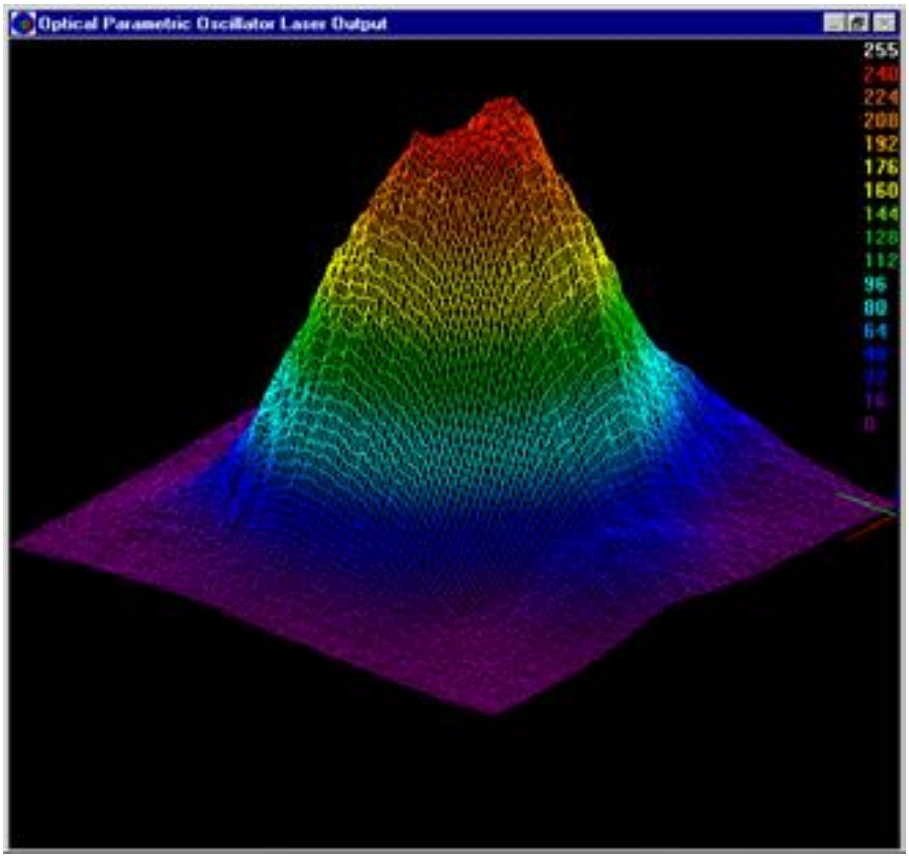

Figure 1.4-A Deformed Gaussian beam, where the power is imperfectly distributed along the axis of propagation

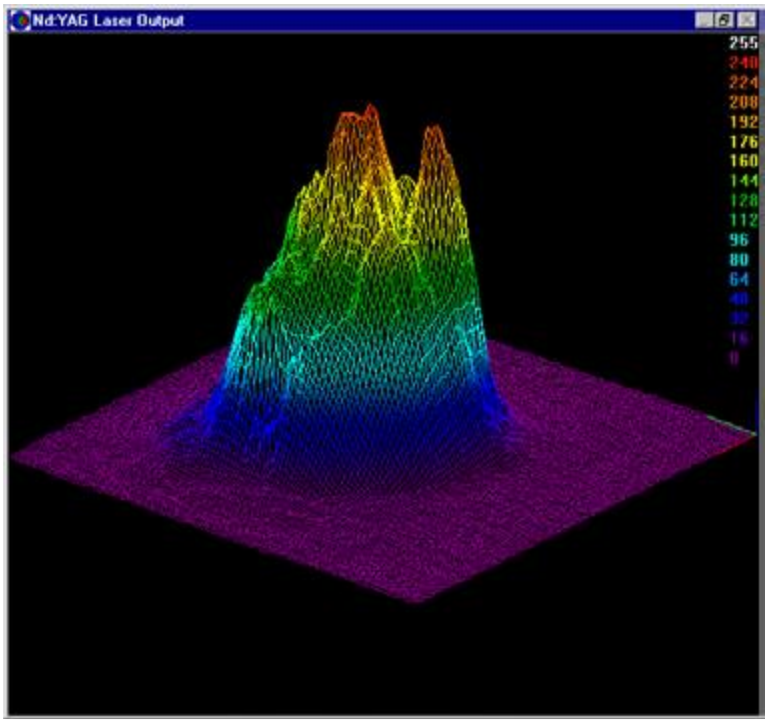

Figure 1.4-B Deformed Gaussian beam. This deformation is known as structured beam, where the energy distribution is out of order and keeps fluctuating along the propagation plan. Much of the energy fades away from the central lobe

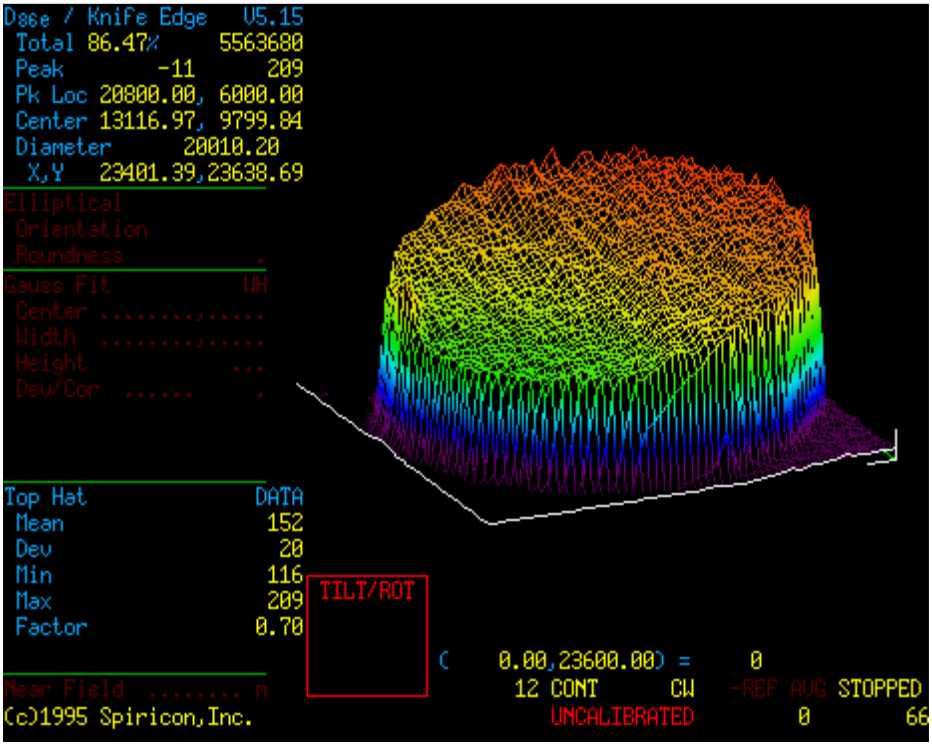

Figure 1.4-C Tilted flat-top beam. In this deformation, the energy is focused on one edge and this doesn't give uniform illumination as intended and will impair the process for which it is being applied

Due to the presence of such a variety of laser beams quality parameters, it is necessary to find a way to measure the laser profiles to make sure the distortion is within the acceptable limits and doesn't impact the performance of the device for which it is designed. It is important to highlight that the type of beam Profiles of interest in this study is the Gaussian Beam demonstrated in figure 1.2.

1.2 Applications of Lasers

Lasers are used in a wide range of applications, including yet not limited to industrial and medical, and military applications. They are even used in the applications that we use on our home daily, such as compute laser mouse and printers.

- Medical Applications There is an amble of medical applications of lasers; one of them is the Photorefractive Keratotomy, in which a flat-top beam is used to make vision modifications to the iris to correct the vision. If the laser devices are not perfectly aligned and there is a 50% tilt in the flat top, the correction to the eye may be 4 dioptres on one side of an iris, with only 2 dioptres on the opposite side. Only a perfectly flat top laser can deliver the expected results, whereas the tilted beam in figure 1.4-D can cause the patient to have an irreversible vision impairment after the operation. Moreover, the flatness of the beam is critical in numerous types of surgeries, such as the removal of port wine stains as well as Tissue cutting and welding. Many medical applications use fiber optics systems and the efficiency of these systems strongly depends on the alignment of the laser beam into the fiber.

- Communication Applications As the information age advances, the need for a high bit rate communication methods gained particular importance. Lasers allow the transmissions with high speed. They are used as carriers in optical communications and there is a wide range of modulation techniques that allow the engineers to maximize the bitrate. The four main modulation techniques are based on amplitude, phase, frequency, and polarization modulations. Only perfect lasers can be used to sustain its properties through long distances. It is necessary to highlight that the long distances particularly impact the beam divergence parameter as the laser beam starts to spread away as it travels.

- Military Applications Most modern weapons rely on lasers to improve aiming accuracy. As an example, the very basic technique is based on a laser telemeter that measures the distance to the target and adjusts the sight based on the distance measured to compensate for the long distance movement of the projectile. The military applications of laser include target designation for guided ballistics.

1.3 Beam Measurement Techniques

As mentioned earlier, the uniformity, stability, and mode pattern of a typical laser used in instruments greatly impact the performance of the devices. A slight misalignment of the collimating optics, for example, will deteriorate the instrument performance. Much of the energy fades away from the central lobe in leaky lasers. As a result, several techniques have been developed to measure the quality of the emitted beam. These techniques are classified into several classes, of which we will encounter the non-electronic methods, electronic methods, and the scanning aperture techniques. This study is dedicated to the scanning aperture technique known as the knife-edge technique, yet we will have an overview of the other methods first.

1.3.1 Non-Electronic Methods

There are several non-electronic methods to measure the laser beam profile. They have been used as early as the lasers were invented. The first of these is the observance of a laser beam reflected or diffused from a wall or other object. It is the simplest and most economic method to measure and observe a laser beam profile. The advantage of this method is that the human eye is logarithmic and can detect vast orders of magnitude difference in light irradiance. However, the human eye can only distinguish 8-12 shades of grey. Consequently, it is almost impossible for visual inspection of a laser beam to provide a quantitative measurement of the beam size and shape. As a result, the beam width measurement by eye may have as much as 100% error.

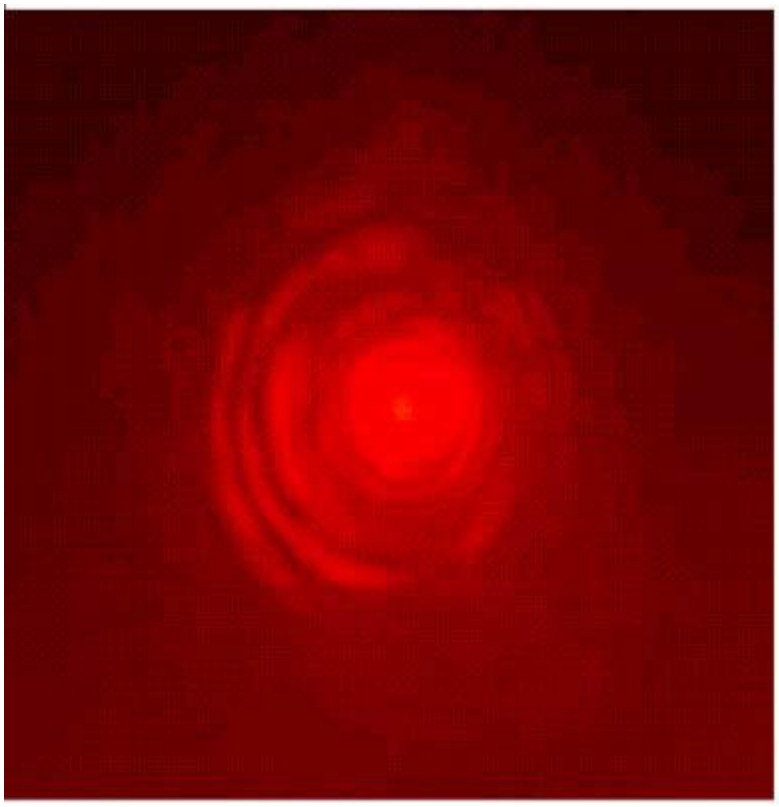

Figure 1.4 He-Ne Laser spot reflected off the wall

Burn paper and Polaroid film are also used for making beam profile measurements. The burn papers typically have a dynamic range of 3, which are unburned paper, blackened paper, and paper turned to ash. Even the most skilled operators can differentiate among more levels, and give a dynamic range of 5. The main disadvantage is that the spot size is highly subjective to the time of exposure of the laser. With longer exposures, the center may not change, but the width of the darkened area will change ±50% or more. Sometimes the depth and the shape of the burn give additional insights into the beam profile. However, this measurement system is obsolete, non-quantitative, and subjective to the capability and experience of the operator. Consequently, this technique is quite unreliable.

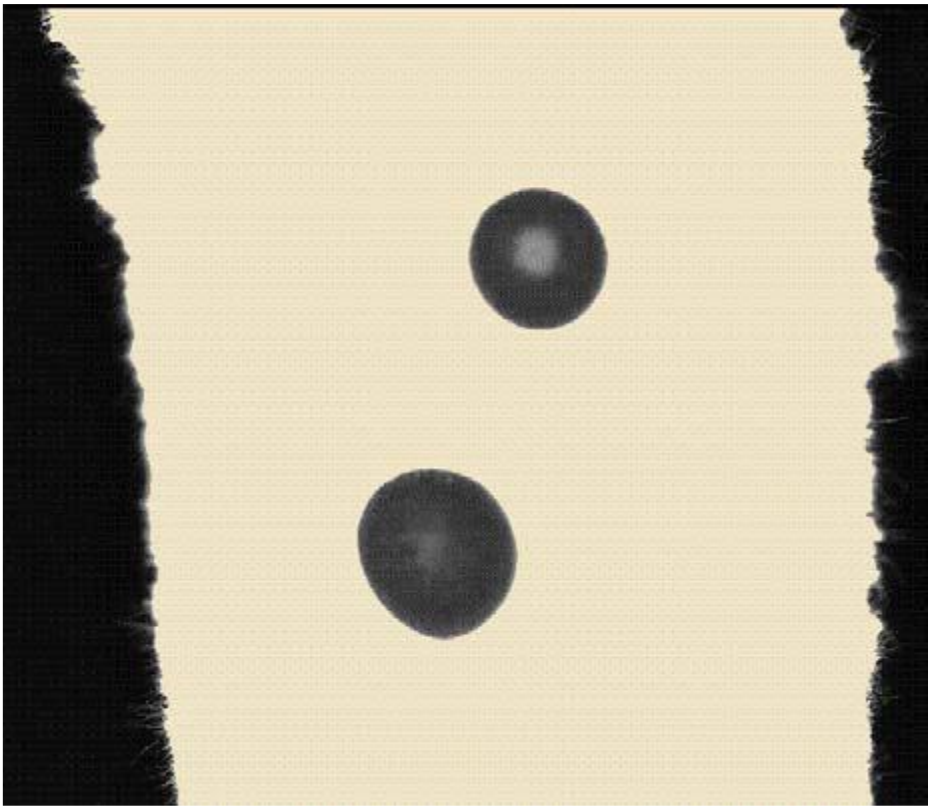

Figure 1.5 Laser beam burns spots on a paper

A more realistic way to image the laser beam on its path is the acrylic burn. It burns a replica of the laser beam profile into an acrylic cube. The shape of the burns demonstrates the profile of the beam. It is even possible to see the mode structure. However, the acrylic mode burns are not real-time. This does not enable us to see to check the time-dependent fluctuations in the laser beam. These time-dependent fluctuations are quite common in the CO2 laser particularly. Moreover, the resulting fumes from the burning acrylic block the incoming laser beam and prevent it from shaping the cube as shown in figure 1.6, where we can see a notch at the top of the beam. It is necessary to place a fan close to the cube to ventilate and clear a path for the laser and avoid the effect of the fumes blocking the laser and forming a non-realistic shape of the beam. Furthermore, the fumes from burning acrylic are toxic to humans.

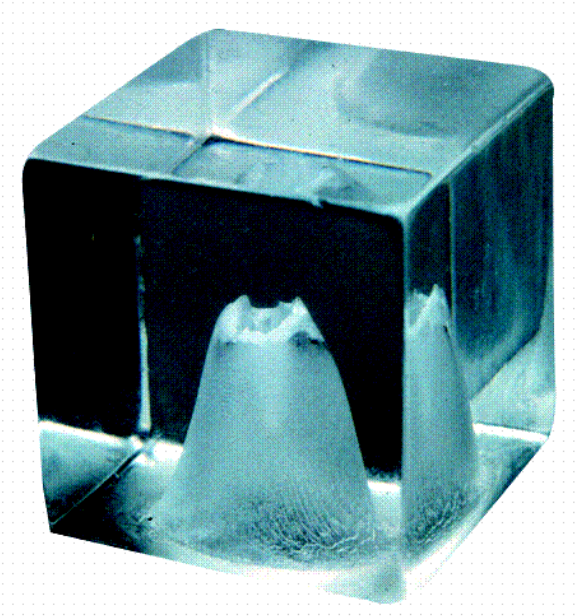

Figure 1.6 Laser Beam burns into an acrylic cube.
the groove on the top is the result of the fumes blocking the beam

1.3.2 Electronic Measurement Methods

In these methods, there is a receiving device used to measure the power of the incident laser beam using electronic analysis. It is necessary, in almost all methods, to attenuate the laser beam to a tolerable level before exposing the measuring device to the beam; otherwise, the device will breakdown thermally. This degree of attenuation depends on two main factors:- - The irradiance of the measured laser beam.

- The sensitivity of the beam profile sensor.

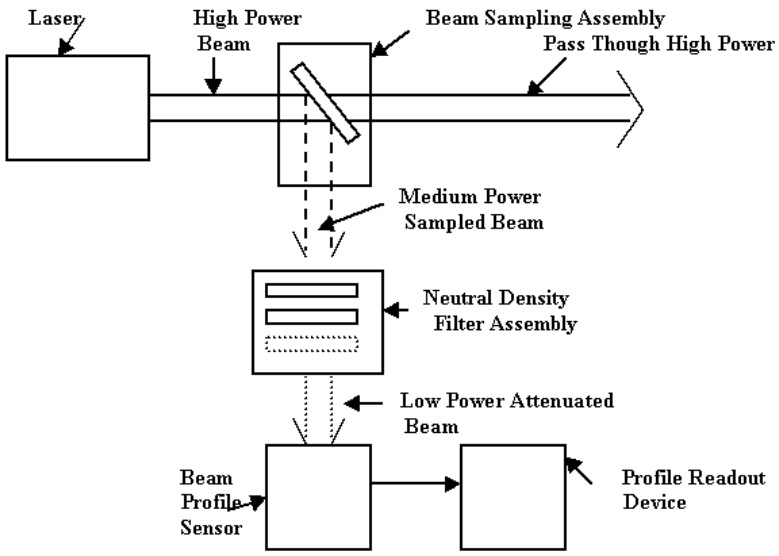

Figure 1.7 Typical setup where a minimum attenuation is required before the sensor measures the beam

It is necessary to mention that some beam profiling sensors can be placed directly into the path of high power beams in the order of 10kW and even greater. For most mechanical scanning devices, the beam sampling assembly is sufficient to reduce the power of the signal to the safe levels. If the original laser beam is already in the safe range, then the scanning device can intercept the beam directly without power reduction. The mechanical scanning instruments can be placed directly in the path of medium power beams because they consist of a single element detector with a rotating drum reflecting or absorbing the light from the sensor during most of the duty cycle; consequently, low power clears its way to the sensing element. In some cases, the beam power is still too high even after the reflection from one sampling surface and it would burn the sensor. In this case, a second reflective surface is implemented to further reduce the beam power before the imaging process.

1.3.3 Mechanical Scanning Instruments

One of the most effective methods used to measure the laser beam profile electronically is a mechanical scanning device. It usually consists of a rotating drum containing a knife-edge, slit, or pinhole that moves in front of a single element detector. This method provides excellent resolution, as small as1 μm. The limit of resolution is set by diffraction from the edge of the knife-edge or slit, and roughly 1 μm is the lower limit set by this diffraction. These devices can be used directly in the beam of medium power lasers with little or no attenuation because only a small part of the beam is hitting the detector element at a given amount of time. The mechanical scanning methods work only on continuous-wave lasers and not on pulsed lasers to avoid the dilemma of synchronizing the movement of the edge and the pulses of the laser. These beam profile instruments can function properly for the visible, UV, and infrared wavelengths by using the suitable type of detectors for the sensor. Additionally, software has been developed to provide illuminating beam profile displays as well as detailed quantitative measurements from the scanning system. This software now exists in the PC-based Windows operating system for easy use. Figure 1.8 demonstrates a commercial version of the knife-edge scanning slit beam profiling instrument while Figure 1.9 shows a typical Windows computer readout. Figure 1.10 illustrates a commercial version of the knife-edge scanning slit beam profiling. Figure 1.10 illustrates a typical mechanical diagram of a scanning slit beam profiler.

Figure 1.8 A commercial scanning edge device

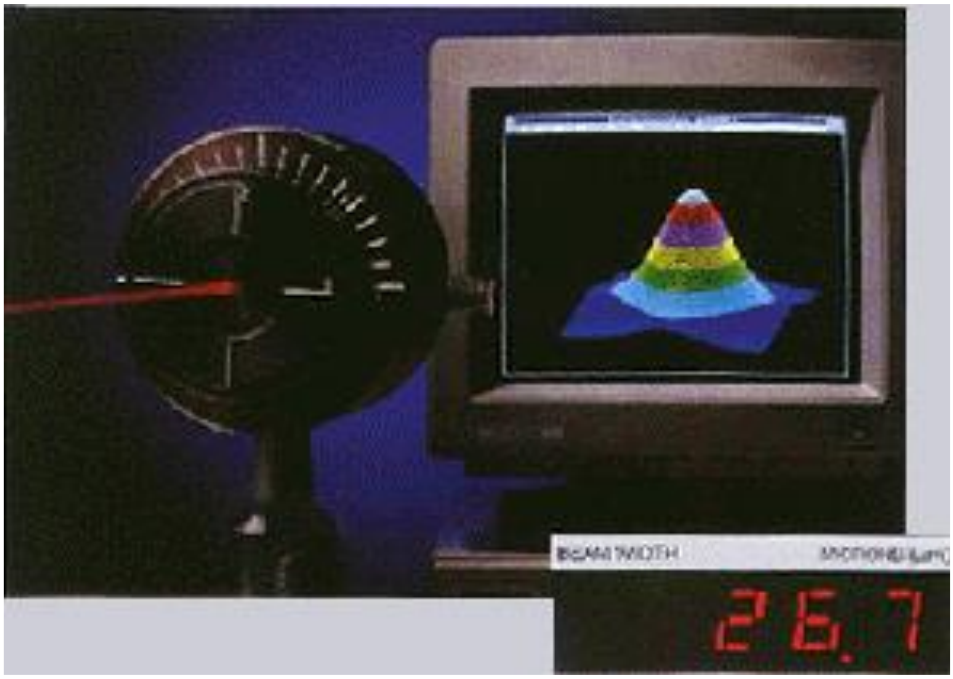

Figure 1.9 Windows of the software used for the scanning edge

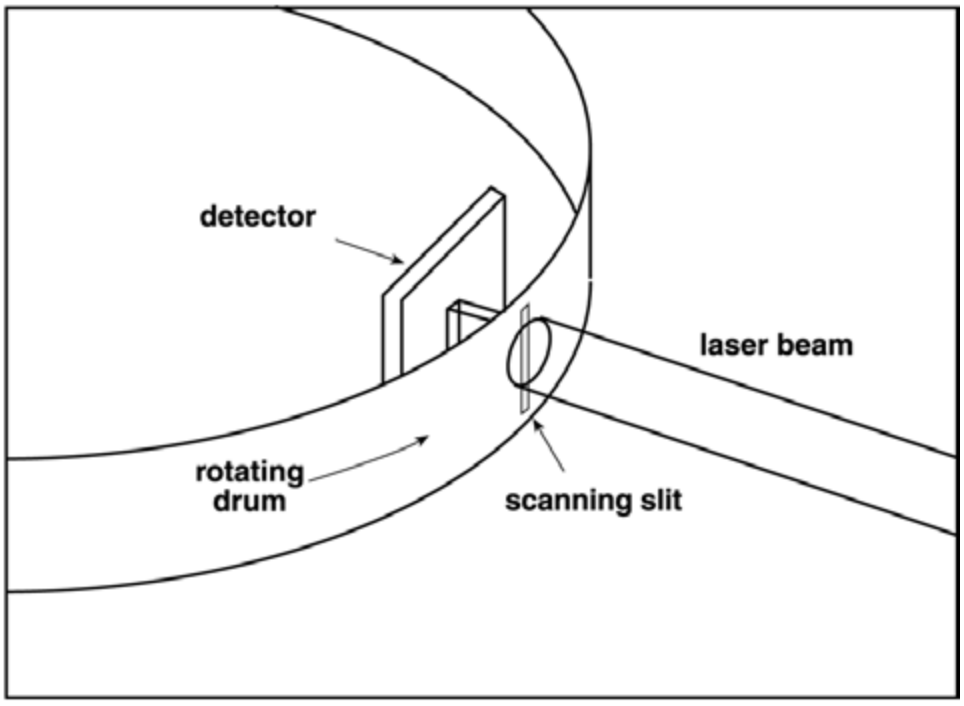

Figure 1.10 Schematic description of the scanning slit technique

1.3.4 Camera-Based Systems

The beam imaging techniques technique is quite simple. It is based on attenuating and shining the laser onto a Charged Couple Device (CCD) camera and measuring the beam profile directly. Due to their simplicity, the beam imaging techniques are the most popular for beam profiling. It can be done using a silicon CCD camera, which has a pixel size of up to a few micrometers and is sensitive to a

wide range of wavelengths from the deep UV (200 nm) to the near-infrared (1100 nm). This range of wavelength corresponds to a broad range of laser gain media. The advantages of beam imaging techniques are:-

- High dynamic range, the CCD chip of a webcam has a dynamic range of around 2^8 to 2^{10}.
- High Resolution down to 4 μm, depending on the pixel size
- CCD cameras with trigger inputs can capture beam profiles of low-duty-cycle pulsed lasers

The disadvantages of the CCD camera technique are:-

- Attenuation is necessary in case of high-power lasers
- The sensor size is limited to about 1 inch.
- CCDs are vulnerable to blooming when used near the edge of their sensitivity.

1.4 Scanning Aperture devices

The most common scanning aperture techniques are the pinhole analysis, the scanning-slit profiler, and the knife-edge technique. The pinhole analysis technique is used to recover the power profile of the laser beam without beam perturbing optics. It is based on an electromechanically actuated translational pinhole mounted on a profiler. This technique requires very narrow steps in both directions of the electro-mechanic translator to achieve a high resolution in the profiling process. This however will shorten the lifetime of the profiling instrument. Several techniques have been suggested to overcome this obstacle. One of them is using digital spatial light modulator based beam profilers, which is done by a **D**igital **M**irror **D**evice (DMD) and a **L**iquid **C**rystal **D**isplay (LCD). This device is advantageous as the DMD is polarization indifferent and operates fast and the LCD based profiler can profile large beams in addition to its longer reliable lifetime thanks to the non-moving parts technology. As shown in figure 1.11, the DMD is exploited to create virtual pinholes on selected zones while the photodiodes 1 and 2 are set symmetrically along the optical axis. The software-controlled virtual pinhole can move along the zone, sampling the power profile of the incident laser beam and forming the pinhole profiler. It is important to use two photodiodes to normalize the detected power in case if laser power fluctuates during profiling operations. The DMD can provide nearly one million pinholes for beam profiling.

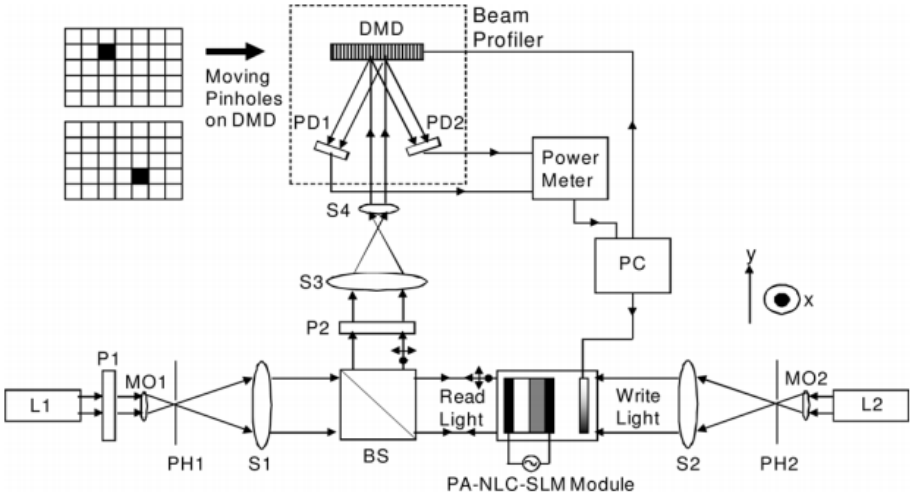

Figure 1.11 DMD-based pinhole laser beam profiling system with an arbitrary beam generator . L1/L2: Lasers. P1/P2: Polarizers. MO1/MO2: Microobjective lenses. PH1/PH2: Pinholes. S1/S2/S3/S4: Spherical lenses. BS: Beam splitter. PD1/PD2: Photodetectors. PC: Personal computer.

The knife-edge technique is based on a blade that intercepts the laser beam and is followed by a photodiode used to measure the incident power corresponding to the blade position. The Scanning-slit profiler uses a thin wire rather than a single knife edge. In which case, the intensity is integrated over the slit width and the resulting measurement is equivalent to the original cross-section convolved with the profile of the slit. These techniques depend on power measurement and it allows the high-resolution measurements down to the submicron regime as well as large beams in the order of few tens of centimeters. However, they do not function for pulsed laser sources as a result of the complexity of synchronization between the aperture motion and the laser pulses.

We can conclude this chapter by that there is an amble of techniques used to perform the laser beams measurements. The most effective as well as the least complex ones are the ones of the scanning apertures and particularly the knife-edge technique. This thesis focuses mainly on demonstrating the knife-edge scanning technique to measure the Gaussian Beams. It will start with a brief review of the Gaussian beam propagation and mathematics, and continue to the rigid statistical analysis of the added noise figures to the samples and end up with the conclusion of a numerous group of experiments.

References

Roundy, C. B. (1990 Jul) The importance of beam profile. Physics World.

Roundy, C. B. (1994 Mar) Instrumentation for laser beam profile measurement. Industrial Laser Review.

Roundy, C. B. (1996 Apr) Practical applications of laser beam profiling. Lasers & Optronics.

Roundy, C. B. (1996 May) Electronic beam diagnostics evaluate laser performance. Laser Focus World.

Roundy, C. B. (1997 Jan) PC-based laser analyzers: New uses require improved devices. Photonics Spectra.

Roundy, C. B. (1994 Oct) Laser-assisted radial keratotomy. Photonics Spectra.

Roundy, C. B. (1996 Aug) Applying beam profiling to industrial lasers. Lasers & Optronics, supplement to Metalworking Digest

Roundy, C. B. (1982 Jan) Pyroelectric arrays make beam imaging easy. Lasers And Applications

Roundy, C. B. (1993 Oct) Digital imaging produces fast and accurate beam diagnostic. Laser Focus World.

Roundy, C. B. (1996 Dec) 12-bit accuracy with an 8-bit digitizer. NASA Tech Briefs.

Roundy, C. B., Slobodzian, G. E., Jensen, K., & Ririe, D. (1993 Nov). Digital signal processing of CCD camera signals for laser beam diagnostics applications. Electro-Optics.

Sasnett, M.W. (1989) The physics and technology of laser resonators, D. R. Hall and P. E. Jackson, eds., Adam Hilger, NY.

Sasnett, M.W. (1993 Aug) Beam geometry data helps maintain and improve laser processes. (Part 1) Industrial Laser Review

Sasnett, M.W. (1994 May) Beam geometry data helps maintain and improve laser processes. (Part 2) Industrial Laser Review

Sasnett, M.W. (1990) Characterization of laser beam propagation. Coherent ModeMaster Technical Notes.

Siegman, A. E., (1986) Lasers, University Science Books, Chapter 7, p. 697.

Carts, Y. V. (1989, Aug). Excimer-laser work spurs UV beam-profiler development. Laser Focus World.

Darchuk, J. (1991, May) Beam profilers beat the laser-tuning process. Laser Focus World.
Forrest, G. (1994, Sept) Measure for measure (Letters). Laser Focus World.

Chapter 2: Mathematics of the Knife Edge Technique and Gaussian Beams

In this chapter, we will review the mathematics of a Gaussian laser beam. Then explain the physics behind the knife-edge experiment and its settings and demonstrate the data analysis adopted.

2.1 Gaussian Beam Calculations

The Gaussian beam is known as the fundamental mode TEM_{00}. It is the solution of the electromagnetic field in the optical resonator. For a Gaussian laser beam propagating along the z-axis, the transverse profile in the x-y plane of the optical intensity distribution is described by the 2-dimensional Gaussian function

$$I(x,y) = I_o \exp\left[-\frac{2(x-x_0)^2}{w_x^2} - \frac{2(y-y_0)^2}{w_y^2}\right] \qquad \left[\frac{w}{m^2}\right] \qquad 2.1$$

Where we have that I_0 is the maximum intensity amplitude (watt/m^2),

w_x and w_y are the $1/e^2$ half widths in the directions of x and y respectively. It can be also defined as the points at which the intensity is decreased to 13.53% of the peak intensity,

and x_0 and y_0 are the coordinates of the center of the beam where there is the peak intensity.

For an ideal Gaussian beam, there exists symmetry among all directions of the beam and its sections are considered circular. Thus, it is a valid assumption to consider a standard beam width as $w = w_x = w_y$

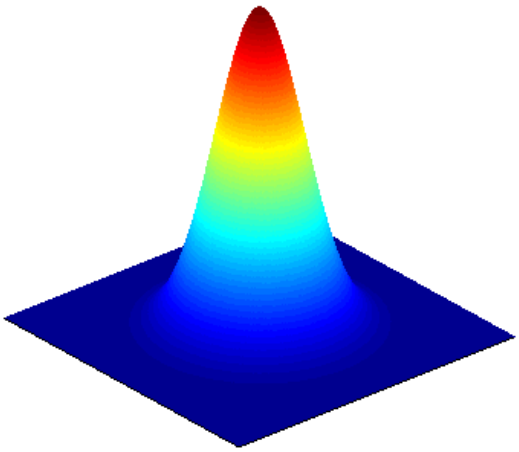

Figure 2.1.a

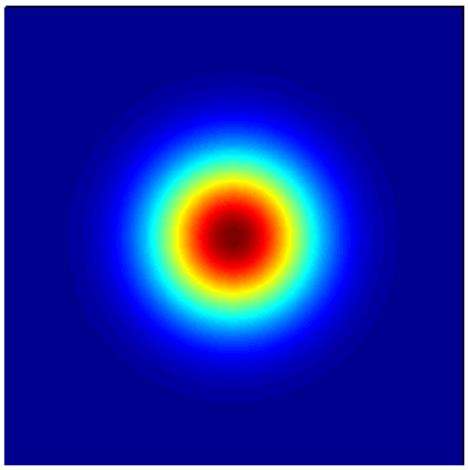

Figure 2.1.b

Figures 2.1.a and 2.1.b side and top views of the Gaussian beam, where the intensity is at the climax at the center and decreases exponentially to reach zero while moving away from the center

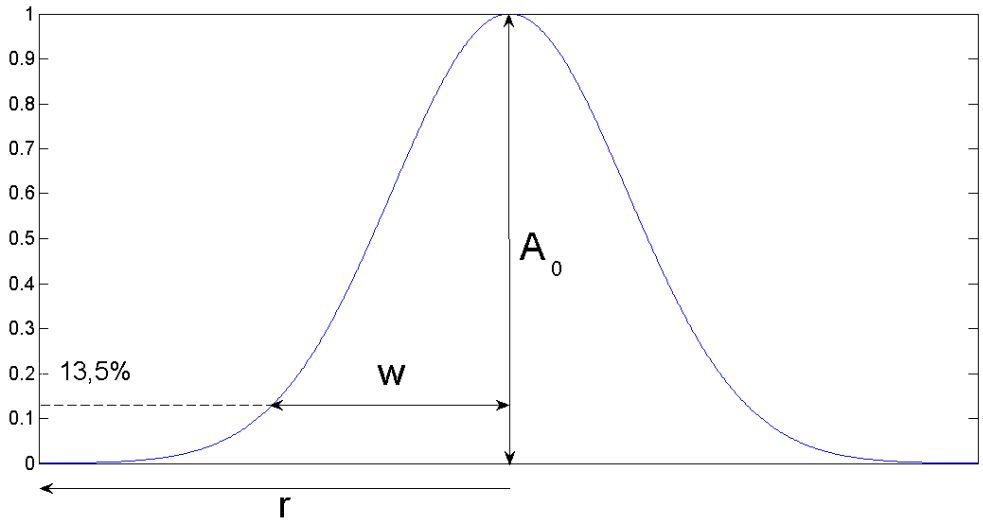

Figure 2.2 A Gaussian beam with the basic parameters A_o and w, which correspond to the maximum amplitude and the beam width respectively

The intensity of the optical laser power received depends directly on the total power P and inversely on the area of the laser beam as

$$A_o = \frac{P}{A} = \frac{P}{0.5\pi w^2} \qquad \left[\frac{w}{m^2}\right] \qquad 2.2$$

, where A is the area of the beam. As shown in figure 2.3, the radius of the beam varies during the propagation process. There are two radii of particular interest that are:-

- The beam waist, which is located at the position where we have the smallest radius, w_o.

- The Rayleigh's range, which is located where the beam area is twice as big as the beam waist and it is commonly referred to as Z_R.

The beam waist and the Rayleigh distance are related as

$$w = w_o\sqrt{1 + \left(\frac{z - z_1}{z_o}\right)^2} \qquad 2.3$$

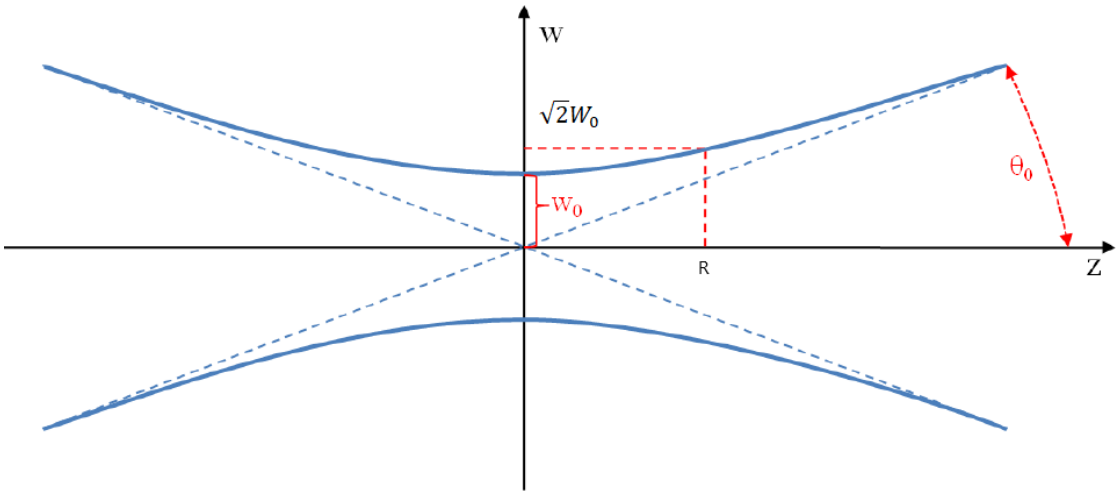

Figure 2.3 Laser beam radius changes as a function of the propagation distance z

During the process of propagation, there are the following invariants:-

$$w_0\theta_0 = \frac{w_0^2}{z_0} = \theta_0^2\, z_0^2 = M^2\frac{\boldsymbol{\lambda}}{\boldsymbol{\pi}} \qquad 2.4$$

Where we have that θ_0 is the beam divergence

$\boldsymbol{\lambda}$ is the propagation wavelength, and

M^2 is a parameter that measures the laser radiation quality.

The term $w_0\theta_0$ is called Beam Product Parameter (BPP) and its minimum value is given by diffraction limit. For the ideal case, M^2 equals 1 and it means that we have an ideal Gaussian beam. Usually, lasers have the M^2 parameter greater than 1 and this corresponds to low laser quality and more deviation from the ideal Gaussian beam. This usually occurs due to non-homogeneity, diffraction losses, the laser type, laser power, or a combination of all.

2.2 Knife Edge Method

This type of measurement technique is based on placing a blade in front of the laser beam and measuring the power transmitted after the blade using a photodiode. In this paragraph we will discuss this technique in detail, mentioning the conditions of the experiment and its conclusions.

2.2.1 Experimental Settings

The beam quality plays a key role in many laser applications. It determines the smallest possible area of the beam at the focal point. The parameter M^2, as mentioned earlier, determines the quality of the output beam and how close it is to the ideal Gaussian beam. The knife-edge method aims to measure w and M^2. The knife-edge technique is advantageous in terms of simplicity, its validity for a wide range of wavelengths, and the ability to obtain high resolution. The K-E method experiment on the TEM_{00} mode is performed by placing a sharp rectangular object on the path of the laser beam and placing a photodiode after the blade to measure the incident optical power. The blade will be moved through one direction perpendicular to the direction of propagation on predefined steps. The blade must move parallel to the X-Y plane, which is perpendicular to the direction of propagation Z.

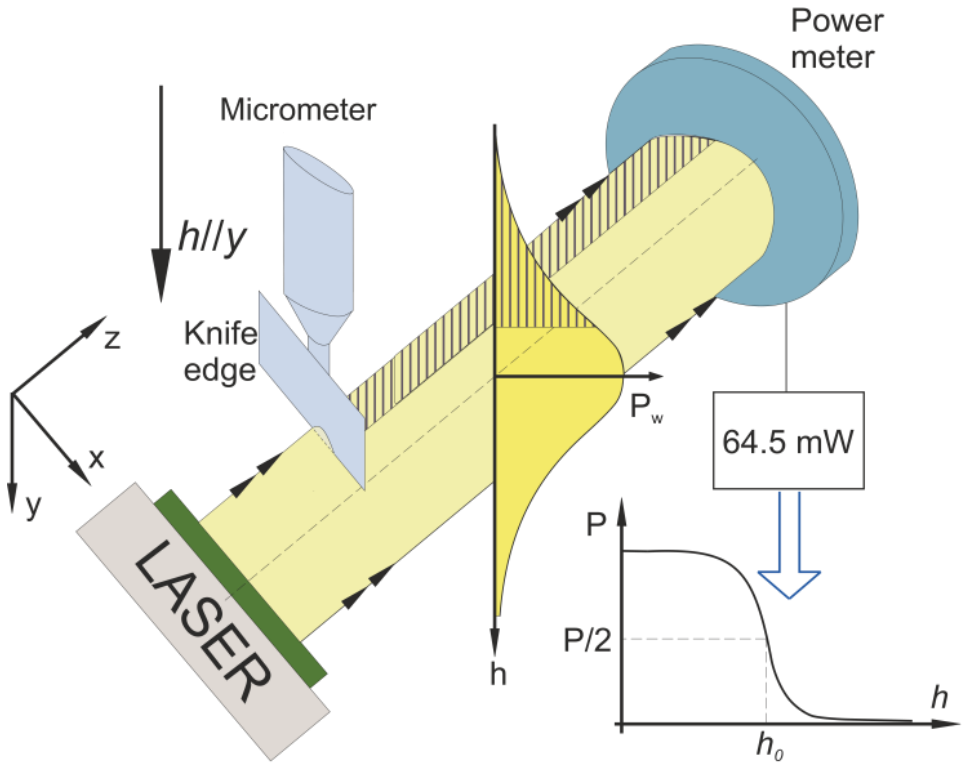

Figure 2.4 Knife-Edge method demonstration

2.2.2 The Mathematics of the Experiment

The power received is at the climax as long as the beam is not covered by the blade and is at minimal when the blade blocks the beam entirely. We measure the full optical power of the laser beam (without intercepting the ray). The measured power at the output of the photodiode is a complementary error function based on the position of the blade as equation 2.5, bearing in mind that the curve of that ERFC is centered around the position $h = h_0$, which corresponds to the position at which the optical power received is at 50% of the expected maximum value.

$$P(h) = \int_{h}^{+\infty} \int_{-\infty}^{+\infty} I(x,y)\ dx\ dy \qquad 2.5$$

$$P(h) = P\frac{1}{2}\left[1 - \text{erf}\left(\frac{h - h_0}{\frac{w}{\sqrt{2}}}\right)\right]$$

$$P(h) = P\frac{1}{2}\,\text{erfc}\left(\frac{h - h_0}{\frac{w}{\sqrt{2}}}\right)$$

The position of h_0 corresponds to standard width of 70.7% of the $1/e^2$ width of the laser beam. More formally, it is defined as $h_0 = \frac{w}{\sqrt{2}} = 0.707w$.

It is important to have a blade long enough to cover the entire horizontal profile of the beam. Having a blade width of 3.3w is enough as the typical photodiode resolution can not be as good as

one-thousandth of the transmitted optical power. It is also important to use a photodiode of matched size in the sense of using a photodiode of radius equal to or greater than the beamwidth. If this solution is not viable, we can use a large numerical aperture lens to collect the optical rays in a small spot matched to the size of the photodiode.

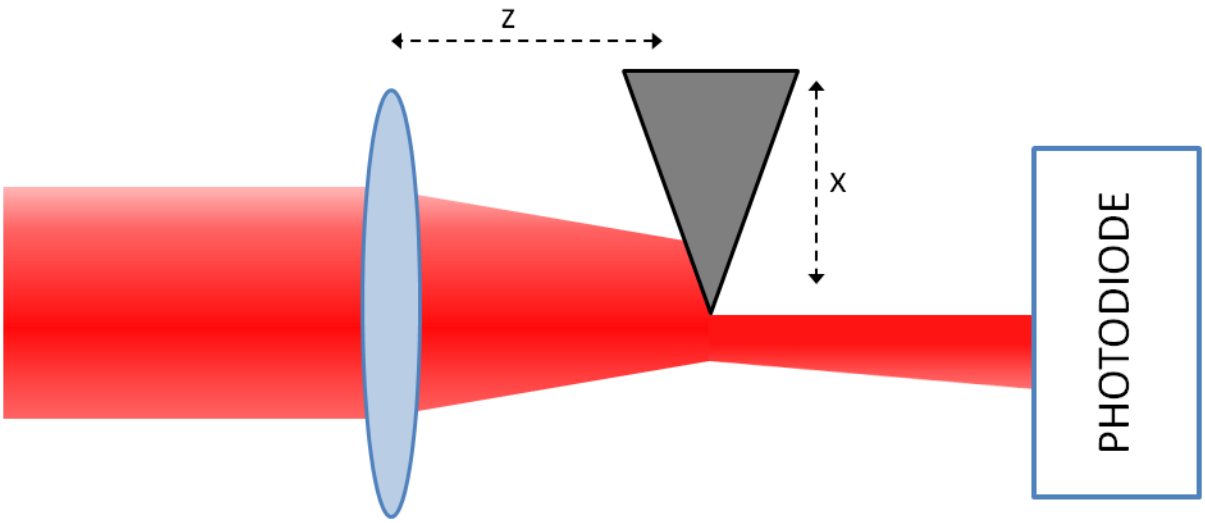

Figure 2.5 Experimental setting in case of using a photodiode with an unmatched size to the laser beam

During the experiment, the blade should be moved carefully on predefined discrete positions and record the optical power received by the photodiode. These minute movements should be performed by the aid of a graded micrometer or a micrometric stepper motor. Then, we record a reasonable number of measurements, ranging from 20 to 100 points, of the received power versus the blade displacement. At that moment, we can plot the data and observing if the two curves of the measured data and the theoretical calculations are matched as shown in figure 2.6.

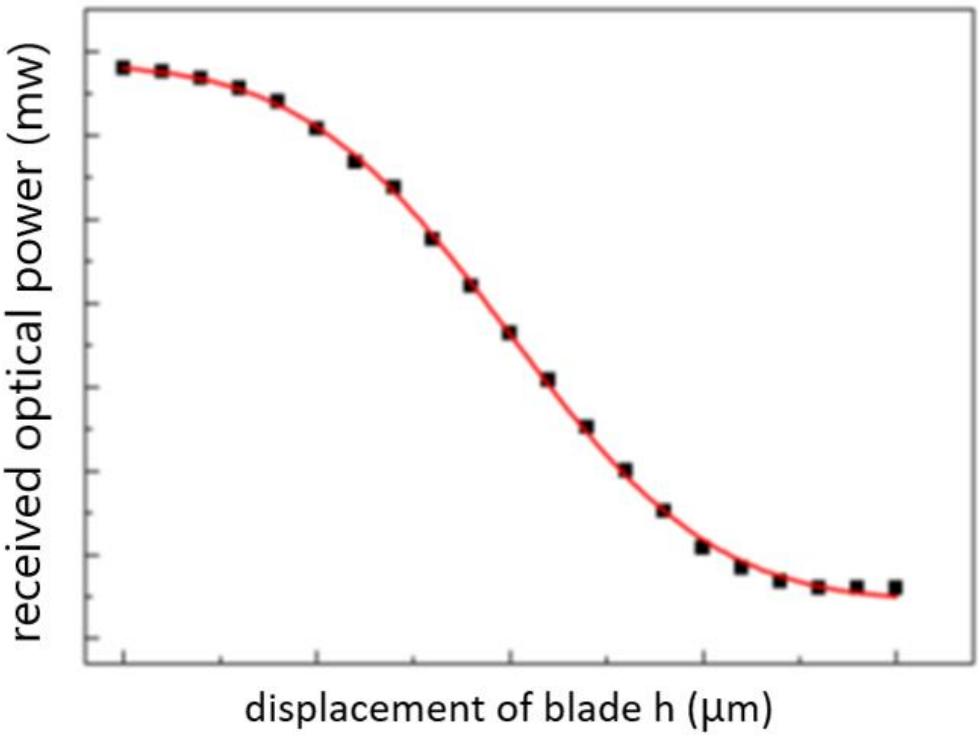

Figure 2.6 Example of the collective graph combining the theoretically calculated received power (solid line) and the actually received optical power by the photodiode during this type of experiment

2.2.3 Plotting the Curve of the Actual Received Power

After collecting the data as shown in figure 2.6, it is necessary to use an algorithm to extract the measured power versus the knife-edge position h, which indicates the spot size of the measured laser beam at the X-Y plane at a particular distance on the axis of Z. the proposed method of data inversion depends on a fitting algorithm that is implemented in MATLAB, Origin R, and MS-excel. This yields an equation involving four parameters as

$$P_i(h_i) = P_{offset} + \frac{P}{2}\, erfc\,[\frac{h_i - h_0}{w/\sqrt{2}}] \qquad 2.6$$

where we have P_{offset} as the background power and it corresponds to the offset power that exists even when the receiver is fully covered by the blade. This offset power exists due to the ambient light or due to the presence of imperfections of the photodiode.

P as the maximum transmitted laser power,

w as the beam radius that is obtained by calculations

h_0 as a position of the blade at which the received power is halved

h_i as the position of the blade

2.2.4 Curves Fitting

Several fitting algorithms can be used to match the curve of measured data to the curve of the theoretical data. This fitting process aims to match equations 2.5 and 2.6 to obtain the parameters P, P_{offset}, h_0, and w. From now on these four parameters will be called Amplitude, offset, center, and width, respectively. The purpose of the entire process is to obtain the uncertainty of the width parameter, which is the laser beam spot size. The fitting process can be easily performed with a simple excel spreadsheet to evaluate the least-squares values of the four parameters by summing the squared differences among the actually measured data and the theoretical model. The excel solver add-on allows getting values closely comparable to the ones obtained by the non-linear fitting on MATLAB. However, it is preferred to use the MATLAB as it can contain powerful mathematical functions as well as its ability to nest several for-loops, which will allow the fine evaluation of the uncertainty sensitivities. The function of the MATLAB used to fit the data was the *NonlinearLeastSquare.* It resolved the direct data numerical inversion of the measured results situated on the calculated theoretical data of equation 2.6. These powerful tools facilitated the calculations of the four parameters we were targeting in this research, which are Amplitude, offset, center, and width.

2.2.5 The Experiment Tools

To perform the knife-edge experiment, the researchers used Gaussian lasers sources of the Er: Glass type of wavelength 1.54 μm. It is an infrared laser (invisible to human eyes) and highly absorbed by water particles. During the experiment, the layout demonstrated in figure 2.7 was implemented to measure the spot size. The knife-edge was placed at different positions on the beam direction, using a blade tightly attached to the micrometer translator. The resolution of the micrometer is as precise as Δh_M=10 μm. However, to facilitate the measurements and maintain fast performance the researchers used an experimental resolution of Δh_E = 50 μm. In the next few lines, there will be a brief explanation of the components of the experiment.

- The **laser pump** is used to enlarge the optical power generated in the laser beam. It converts the electrical power to optical power through a process known as population inversion, in which more electrons exist in a high state than those in the lower unexcited energy levels. This concept very important in the science of laser due to its importance

- The **collimation lens (C)**is used to unify the direction of light rays and make them parallel to each other. The collimation improves the quality of the laser by minimizing the divergence angle, minimizing the energy loss, and increasing the spatial resolution. In this experiment, the collimation lens is followed by the knife-edge with a spacing of $\boldsymbol{d_P}$**=2 mm**.

- The **focal lens (F)** is used to concentrate the laser rays on the Yb-Er-glass Active Medium **(AM)**, which is used to generate the second laser beam.

- An optical power meter is a photodiode. In this experiment, the researchers used a large-aperture integrating sphere InGaAs calibrated photodetector to measure the laser optical power passing the blade. It has been placed after the output coupler **(OC)** at a distance of d_E = 131 mm

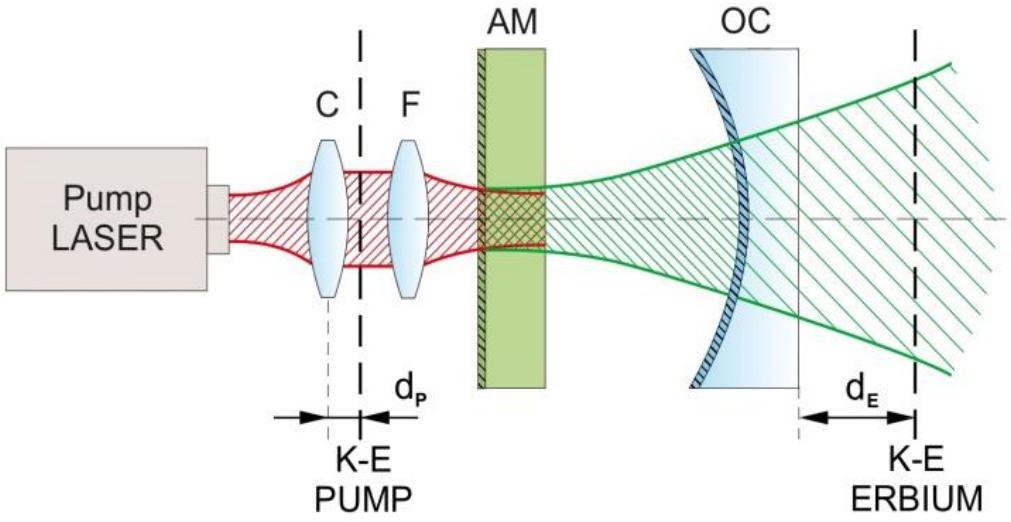

Fig. 2.7 Experimental setup of the pump laser

2.3 Results Acquired and Numerical Analysis

The researchers record the 3-digit numerical value at the power meter output. During the first set of measurements, the researchers measured the laser spot size for a 976 nm fiber-coupled laser diode pumped into Yb, Er:glass laser [erbium]. The laser pump was of commercial source (THORLABS, BL-976PAG) fiber-coupled into a single-mode optical fiber. The output beam passed to a short-focal-length, fiber-coupled, optical collimator (THORLABS, F230APC-980). The output beam of the pump is a pure fundamental Gaussian mode TEM_{00}. This means that its beam quality parameter, M^2 , is almost equal to 1 and its transverse profile is described by equation 2.1. This beam has been analyzed using the knife-edge method in the free space after the collimator as shown in figure 2.7. The researchers performed the measurements of the laser pump without mounting the subsequent erbium laser cavity and the results of the measurements are shown in figure 2.8, where the researchers measured the laser pump power at a distance of 2 mm from the collimator for 61 experimental points and all points are displaced by 50 μm from one another.

The measurements are expected to fit with the theoretical curve given in figure 2.8 and demonstrate a complementary error function as mentioned after properly putting into account the amplitude, offset, center, and width of this curve. The measured data were fit to the theoretical data using MATLAB and particularly the fit function with *NonlinearLeastSquares* option. Figure 2.8 shows the analytical data on the solid curved line and the measured data on the circles. This data fitting process revealed the parameters shown in table 2.1, where column A demonstrates the data fitting obtained by the MatLab nonlinear least-square option while column B demonstrates the results obtained by the solver function in the Excel spreadsheet.

	A	B
$P_{0,P}$	76.36 mW	75.95 mW
P_{offset}	0.253 mW	0.606 mW
$h_{0,P}$	0.6815 mm	0.6815 mm
w_P	405.6 μm	401.1 μm

table 2.1

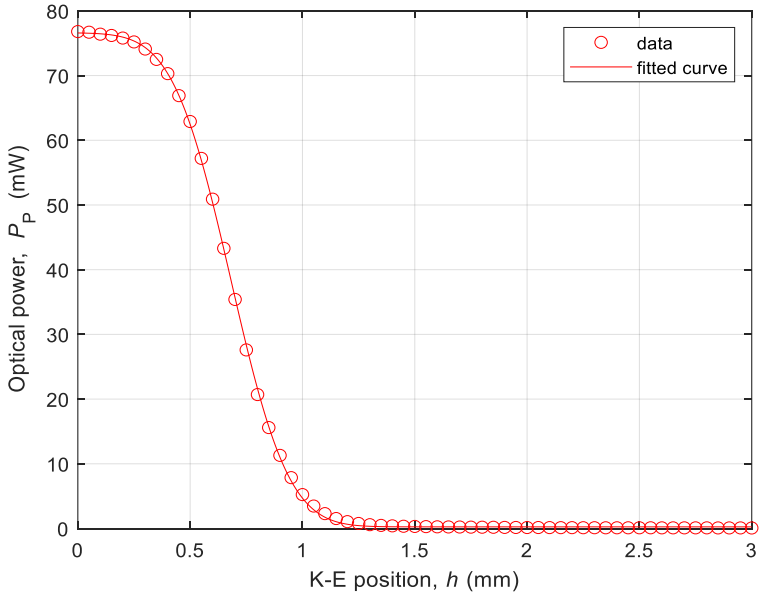

Figure 2.8 Received pump power 2 mm after the collimator using the Knife-Edge method. It indicates the measurements for 61 points spaced by 50 μm from one another

The excel solver doesn't specifically include the uncertainty for the w_P parameter. On the other hand, the Matlab fit function yields a 95% confidence interval of the w_P parameter, as for 400.8, 410.5 μm.
To facilitate the analysis, we can assume expanded uncertainty values for the excel and the MatLab fitting as for $U(w_{P,Excel}) \cong U(w_{P,\,MATLAB}) \cong 5$ μm, using $k=2$ as the expanded uncertainty factor and consequently putting into account the 95 % confidence intervals for normal distributions. This makes the two measurements compatible. The similar uncertainty assumption for different algorithms end programs is still unjustified.

The Knife-edge method and the numerical inversion on the obtained data from the pump laser beam have allowed us to obtain an indirectly measured spot size of approximately 0.4 mm, which is a value with a good match with the calculated beam spot size at the collimator output (SM fiber at 980 nm Fujikura SM98-PS-U25A-H and collimator THORLABS F230APC-980 with focal length 4.55 mm).

The standard uncertainty $u(w_P)$ of the measurements is calculated using direct data inversion based on equation 2.6, which was achieved by a MATLAB fit function. The next paragraphs are dedicated to discussing this process in detail.

In the second group of experiments, the researchers used the Yb,Er:glass laser previously developed in the laboratory. It is end-pumped by the pump laser diode as shown in Figure 2.7. the researchers performed different spot-size measurements at different distances from the laser output mirror. The erbium laser wavelength is around 1.54 μm. The laser beam of the air-coupled erbium-laser is a pure fundamental Gaussian mode TEM_{00} ($M^2_E \cong 1$) and so its transverse profile is well described by equation 2.1. when the distance between the laser spherical output mirror and the knife-edge was d_E=131 mm, we obtained the experimental data shown in figure 2.9, in which the power level of the pump is around 350 mW. To avoid exhaustive over-sampling, it was more effective to divide the 57 sample point as follows

- The first 2 points close to the maximum power are spaced by 500 μm
- The following 46 points are equally spaced by 50 μm- The last nine subsequent points of the measurement are spaced by 200 μm

The numerical fitting of the measured data to the theoretical curve provided by equation 2.6 was done the same way as in the case of the pump laser. It gives the results shown in Figure 2.9. The fitting is again good and the fit parameters are shown in Table 2.2

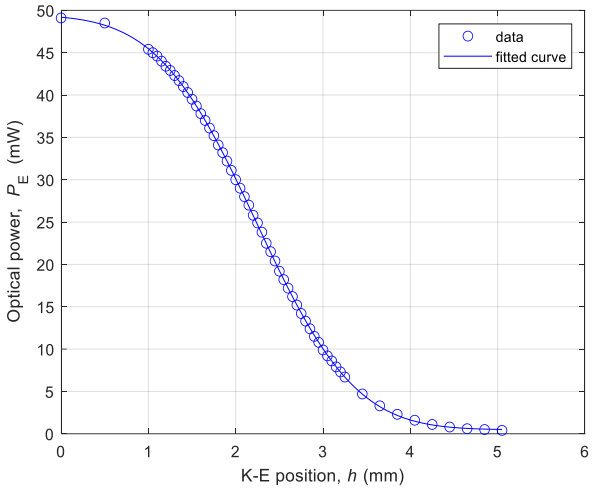

Figure 2.9 Measurements obtained using Yb,Er:glass spaced by d_E=131 mm from the knife-edge on 57 points. Notice the different spacing of the samples depending on the sample position

$P_{0,E}$	49.01 mW
$P_{OFF,E}$	0.4732 mW
$h_{0,E}$	2.236 mm
w_E	1.7777 mm

Table 2.2

The fit function of MATLAB returned a confidence interval of 95 % [1.7678, 1.7862] mm for w_E. As a result, the erbium laser spot size after the collimator is 1.7777 mm. this size, jointly with the two recorded measurements at distances of d_{E-}=125 mm (w_{E-}=1.6916 mm) and d_{E+}=137 mm (w_{E+}=1.8639 mm), is shown in figure 2.10. It evaluates the beam waist for the erbium laser as $w_{0,E}$=34.3 μm within the laser cavity, which is a parameter that is impossible to measure inside the laser cavity since it is located inside the solid active medium, erbium. For the standard uncertainty of our measurement, $u(w_E)$, which the researchers achieved through direct data inversion based on equation 2.6 and performed with a MATLAB fit, we will discuss it in more detail in the next chapter.

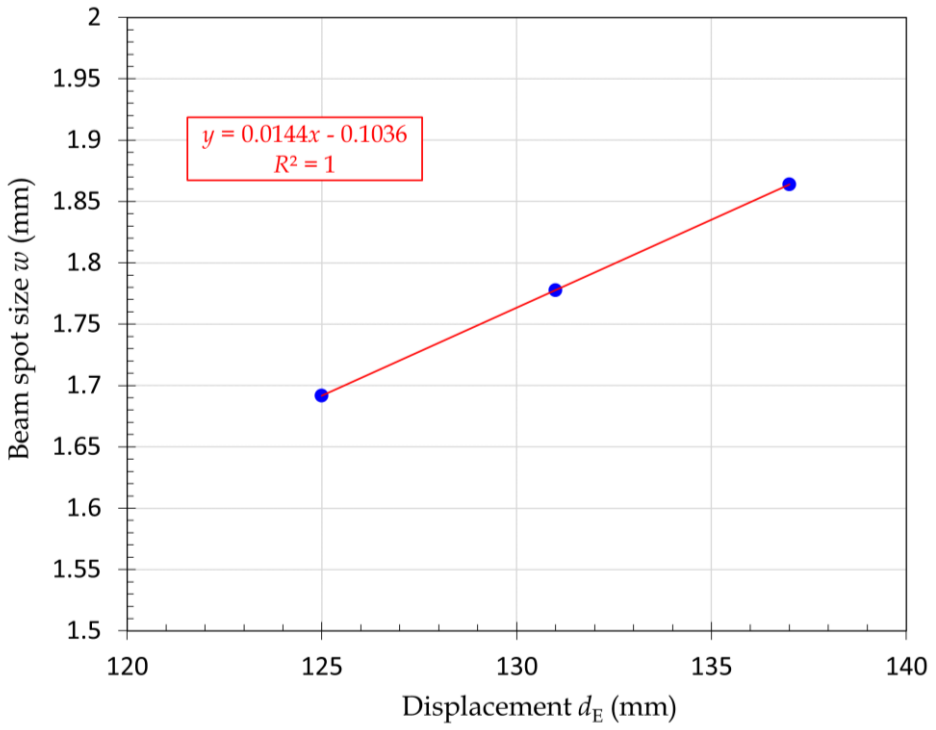

Figure 2.10 Indirectly measured erbium-laser spot sizes as a function of the displacement from the laser output mirror. These points are obtained by a K-E measurement, and the corresponding non-linear fit in the *x*-*y* plane, at distance d_E from the laser mirror. Values within the box represent the linear fit of the 3 experimental points in the divergence region (far-field)

References

W. Koechner, *Solid-State Laser Engineering*. New York, NY, USA: Springer, 2006. ISBN 0-387-29094-X.G.

P. J. Shayler, "Laser beam distribution in the focal region," *Appl. Opt*., vol. 17, no. 17, Sept. 1978.

T. Baba, T. Arai, and A. Ono, "Laser beam profile measurement by a thermographic technique," *Rev. Sci. Instrum.*, vol. 57, no. 11, Dec. 1986.

K. D. Kirkham and C. B. Roundy, "Current Technology of Beam Profile Measurement," in Fred M. Dickey, *Laser Beam Shaping: Theory and Techniques*, 2nd Ed., Boca Raton, FL, USA: CRC Press, 2017. ISBN 9781138076303

J. A. Arnaud, W. M. Hubbard, G. D. Mandeville, B. de la Clavière, E. A. Franke, and J. M. Franke, "Technique for Fast Measurement of Gaussian Laser Beam Parameters," *Appl. Opt*., vol. 10, no. 12, Dec. 1971.

Y. Suzaki and A. Tachibana, "Measurement of the μm sized radius of Gaussian laser beam using the scanning knife-edge," *Appl. Opt*., vol. 14, no. 12, Dec. 1975.

Chapter 3: Statistical processing and Reduction of the Uncertainty Sensitivities

In this chapter, we will understand the statistical analysis and the model adopted in this experiment with a particular focus on the data inversion method. Then we will understand how using this method reduces the uncertainty in the knife-edge experiment and the parameter that influences the error uncertainty.

3.1 Statistical Analysis

The process of the non-linear fitting of the data to the equation 2.6 makes it possible to analytically evaluate the sensitivities of the measured laser spot size uncertainty $u(w)$ to the uncertainties of the input parameters by repeating the fitting process on several random values of added noise to the input data. The uncertainties that affect the input parameters are:-

- the relative uncertainty of the measured optical power, $u_r(P)$,
- the relative uncertainty of the measured knife-edge position, $u(h)$.

The relative and absolute uncertainties of the two input variables are used due to the influence of the uncertainty that is proportional to the value of the power in the laboratory conditions. On the other hand, the knife-edge position uncertainty is measured with an absolute uncertainty independent from the position value. As a result, it was necessary for the researchers to evaluate $S_{w,P}=(\partial w)/(\partial P)$ and $S_{w,h}=(\partial w)/(\partial h)$ and then, assuming that P and h can be measured independently, it is possible to calculate the uncertainty $u(w)$ as given by equation 3.1

$$u(w) = \sqrt{\left(\frac{\partial w}{\partial P}\right)^2 u^2(P) + \left(\frac{\partial w}{\partial h}\right)^2 u^2(h)} = \sqrt{s_{w,P}^2 u^2(P) + s_{w,h}^2 u^2(h)} \quad (3.1)$$

It is valid to assume that there is no dependence among the measurement of optical power and the measurement of micrometer blade positions since there is no common influencing term. In other words, the pump laser temperature and power are independently stabilized from the ambient temperature and there is no way to affect the power meter precision. In case of uncertainty or noise on the position of the knife-edge, is it possible to calculate it as a constant or absolute uncertainty σ_h at each position step. However, when considering the uncertainty or the noise on the optical power, it is necessary to assume a dominant relative uncertainty$\sigma_{r,P}$. This actually is due to that the optical power is proportional to the measured level of power.

To estimate $S_{w,P} = \frac{\partial w}{\partial P}$ and $S_{w,h} = \frac{\partial w}{\partial h}$, the researchers executed repetitive calculations of adding WGN to each of the measurement points for i running from 1 to n for the nonlinear fitting of the equation 2.6, where i is the experimental point. In the first group of calculations, the researchers add noise on the power values (P_i), with a relative standard deviation$\sigma_{r,P}$, and in the second group of calculations, the researchers add noise on the position, values (h_i), with a standard deviation σ_h. This simulation has been repeated for R times and then statistical analysis is carried out on the vector of R estimated beam widths, w of elements w_j, with j going from 1 to R. Typically R=5000 in these simulations, providing for repeatable results. The obtained vector w allows evaluating the average μ_w and the standard deviation σ_w of the estimated beam width w, for the specific value of added WGN. This procedure has been repeated for several different amplitudes of the input noise (standard

deviation of the added WGN) ranging from 0 to a maximum value of interest, which is up to 5 mW for the power noise and up to 10 μm for the position noise.

3.1.1 The Statistical Analysis of the Pump Laser Measurements

Now we will understand the effects of noise and uncertainty on the optical power of the pump laser (referred to with subscript "P" from now on) for the same experimental 57 points of the knife-edge measurement on the pump laser of Figure 2.8. To do this the researchers have changed the values of $\sigma_{r,P,P}$, which is the relative standard deviation of WGN added to the experimental power values of the pump laser P_i. This allowed them to obtain the spot-size average value, $\mu_{w,P}$, and its standard deviation $\sigma_{w,P}$ as shown in Figure 3.1, in which the average width $\mu_{w,P}$ of the spot-size is estimated incorrectly (with a bias) depending on the noise level $\sigma_{r,P,P}$ added to the optical power and having an increasing dispersion $\sigma_{w,P}$ as the value of the deviation increases. Figure 3.2 shows that the standard deviation of the average estimated spot-size, the uncertainty $u(w_P)= \sigma_{w,P}$, increases linearly by increasing values of $\sigma_{r,P,P}$ in this noise input range. The sensitivity of the measurement uncertainty $u(w_P)$ of the pump laser spot-size w_P, to the pump power relative uncertainty $\sigma_{r,P,P}$ in percentage value ($S_{w,P}$) indicated in equation 3.1, is evaluated as the slope of Fig. 3.2 and in this case, it is $S_{w,P,P}$=4.2 μm/%.

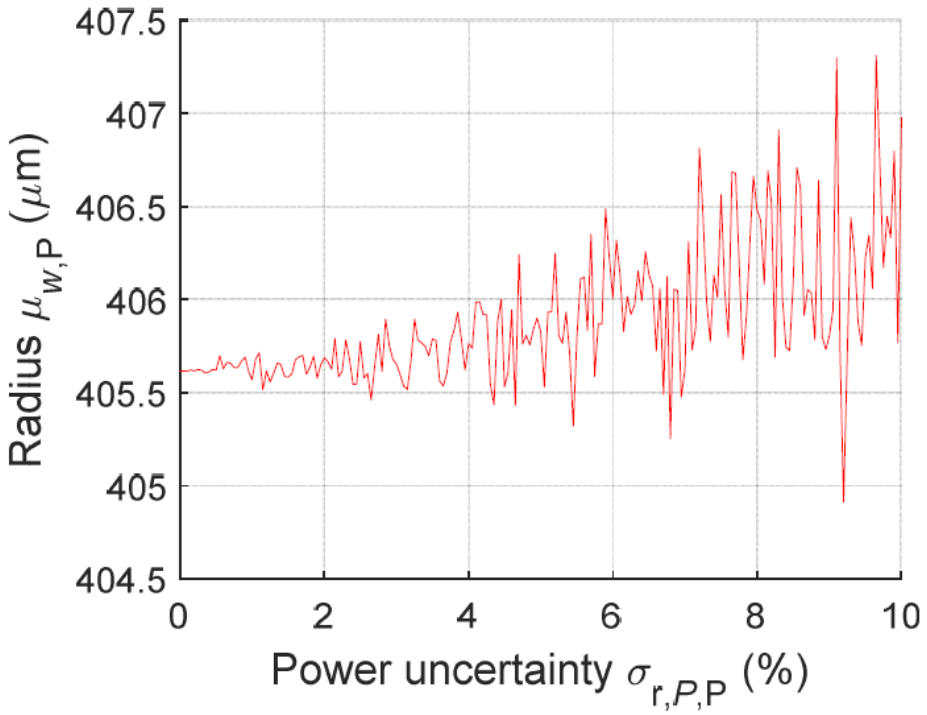

Figure 3.1 Estimated average beam radius in micrometers plotted to the power uncertainty of percentage of the laser beam power of standard deviation σ

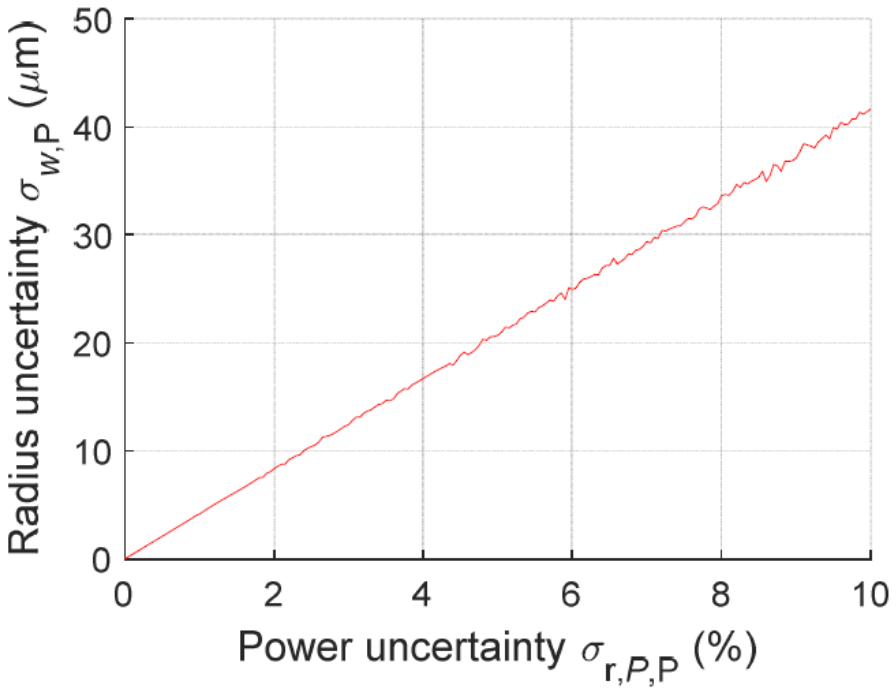

Figure 3.2 Pump laser spot-size uncertainty as a function of noise $\sigma_{r,\,P,P}$ on the pump power

The researchers then studied the effects of noise and uncertainty on the knife-edge position for the pump laser, again, for the same points in Figure 2.8. To do this, they have changed the values of $\sigma_{h,P}$, which is the standard deviation of added WGN on experimental K-E position values (h_i), and obtained the spot-size average value, $\mu_{w,P}$, and its standard deviation, $\sigma_{w,P}$, as shown in Figure 3.3. It shows that the average width $\mu_{w,P}$ of the pump spot-size is evaluated incorrectly (with a bias) depending on the noise level σ_h on the knife-edge position and repeatedly having larger and larger dispersion $\sigma(w_P)$ for increasing values of $\sigma_{h,P}$. On the other hand, Figure3.4 shows that the standard deviation of the average estimated spot-size (the uncertainty $u(w_P)$) increasing directly with the values of $\sigma_{h,P}$ in the mentioned level of noise range. The sensitivity of the measurement uncertainty of the pump laser spot size $u(w_P)$, to the K-E position uncertainty σ_h, $S_{w,P}$ mentioned in equation 3.1 and evaluated as the slope of Figure 3.4 , is, in this case, $S_{w,h,P}$=0.74 μm/μm, which previously was equal to 0.52 μm/μm. It is necessary to understand that the presence of noise on the position values of the K-E makes the laser spot size overestimated, which means that the measurement is biased by an amount increasing directly with the level of position noise. We can observe this clearly if we compare figure 3.3 to figure 3.1 where this error in the estimation is absent. By these calculations performed on the pump spot-size that were measured by the knife-edge technique in the experimental conditions, it is possible to observe 3 important conclusions that:

1P) The spot-size is increasingly overestimated due to the increases in the relative noise on laser power and that the uncertainty increases directly with the input noise.

2P) The spot-size is increasingly overestimated due to the noise on the knife-edge position with increases of uncertainty for an increasing input noise. .

3P) The sensitivities of spot-size uncertainty to the relative noise on power and the absolute noise on position are different. In the experiment, they are $S_{w,P,P}$=4.2 μm / % and $S_{w,h,P}$=0.74 μm/μm, respectively.

The conclusions 1_P and 2_P are surprising and consequently interesting. The presence of noise on the inputs experimental values P_i and h_i lead to a bias error of Δw_p in the measured beam radius w_p. of less than 1 micrometer for a pump laser of spot size 400μm as shown in figures 3.1 to 3.4. Such bias comes from a combination of the input noise and the nonlinear behavior of equation 2.6, in which w is a function of P and h. the conclusion 3_p is relevant when evaluating the combined standard uncertainty of the spot size w and in this case, u(w) is described by equation 3.1. such calculation can be performed after estimating the input position noise u(h) and the input relative power noise $u_r(P)$.

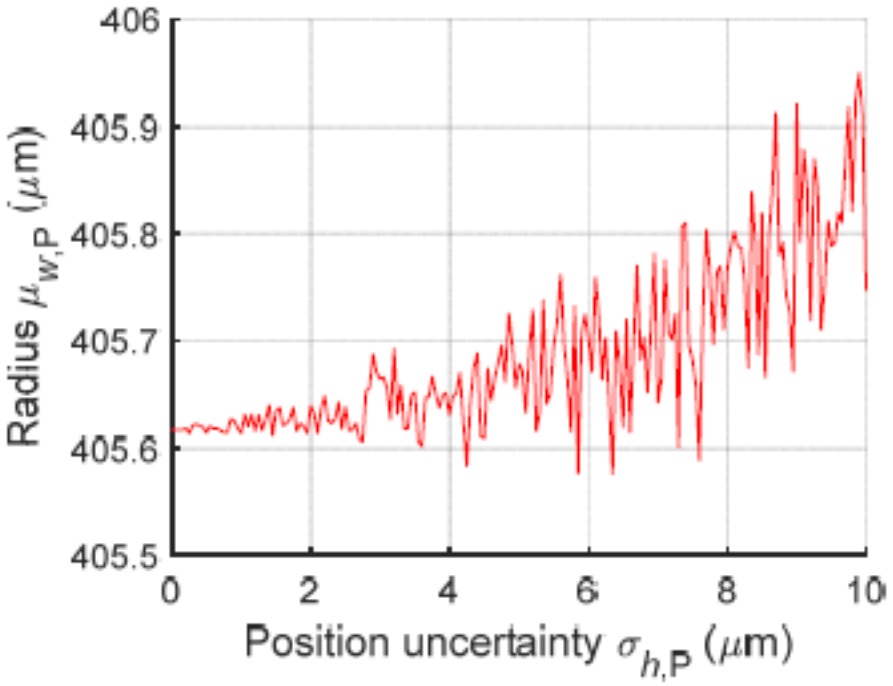

Figure 3.3 Pump laser spot-size average value as a function of noise $\sigma_{h,P}$ on the Knife position

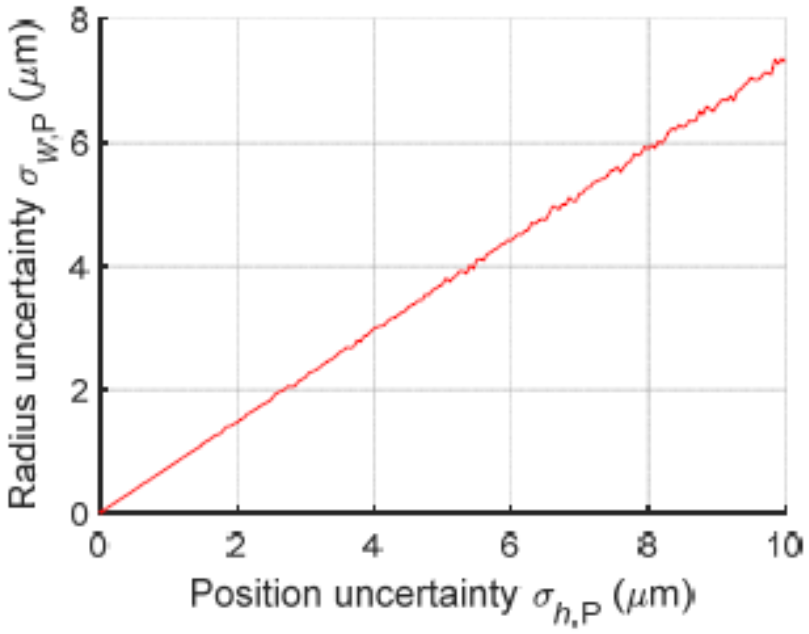

.

Figure 3.4 Pump laser width uncertainty as a function of noise $\sigma_{h,P}$ on the Knife Edge position

3.1.2 The Statistical Analysis of the Erbium Laser Measurements

Later, the researchers studied the effects of noise and uncertainty on the optical power profile of the erbium laser for the same experimental points of the knife-edge measurement on the pump laser of figure 2.9. For this reason, we will use the subscript "E" from now on. For this purpose, it was necessary to alter the values of $\sigma_{r,P,E}$, which is the relative standard deviation of WGN added on experimental power values of the erbium laser. Then, we will understand how to obtain the spot-size average value, $\mu_{w,E}$, as well as its standard deviation, $\sigma_{w,E}$, as demonstrated in figures 3.5 and 3.6.

As shown in figure 3.5, the average width $\mu_{w,E}$ of the spot-size is estimated incorrectly due to the presence noise. For a relative noise level $\sigma_{r,P,E}$ added to the optical power, there is a positive bias in the measured spot size. There is an evidently increasing dispersion $\sigma_{w,E}$ for increasing values of $\sigma_{r,P,E}$. In fact, figure 3.6 shows that the standard deviation of the average estimated spot-size, the uncertainty $u(w_E)$, increases linearly with increasing values of $\sigma_{r,P,E}$ for this range of noise. The sensitivity of the measurement uncertainty of the erbium laser spot size $u(w_E)$ to the erbium laser power uncertainty $\sigma_{r,P,E}$, $S_{w,P}$ indicated in equation 3.1 and evaluated as the slope shown in figure 3.6, is $S_{w,P,E}$=18 μm/%.

After then, the researchers studied the effects of noise and uncertainty on the knife-edge position for the erbium laser using the 57 experimental points shown in figure 2.9. Thus, , it was necessary to modify the values of $\sigma_{h,E}$ and $\sigma_{w,E}$ which are the standard deviation of WGN added to experimental height values and its standard deviation. The spot-size average value, $\mu_{w,E}$, was obtained as shown in Figures 3.7 and 3.8.

Figure 3.7 shows that the average width $\mu_{w,E}$ of the spot-size is estimated incorrectly, biased, depending on the noise level σ_h added to the knife-edge position and, again, having and increasing dispersion $\sigma(w_E)$ directly with the values of $\sigma_{h,E}$. Figure 3.8 shows that the standard deviation of the average estimated spot-size, the uncertainty $u(w_E)$, increments linearly along with increasing values of $\sigma_{h,E}$ when only this contribution is considered. The sensitivity of the measurement uncertainty of the erbium laser spot size $u(w_W)$ to the knife-edge position uncertainty σ_h , $S_{w,P}$ indicated in equation 3.1 and evaluated as the slope of Figure 3.8, is, in this case, $S_{w,h,E}$=0.67 μm/μm previously equals 0.47 μm/μm.

The presence of noise over the blade position causes an over-estimation of the laser spot size by an amount increasing with the value of the added noise. It can be observed if we compare figure 3.5 to figure 3.7, where this error in estimation is absent and also to figures 3.1 and 3.2

The calculations performed on the erbium laser spot-size measured by the knife-edge technique, in the experimental conditions we notice that:

1_E) The spot-size is overestimated (biased) due to increasing the relative noise on the laser power and with larger uncertainty when the input noise increases.

2_E) The spot-size is overestimated tremendously when the noise on the knife-edge position is increased, once again with more uncertainty when the input noise is increasing.

3_E) The sensitivities of spot-size uncertainty to the noise on power and position are different. In this experimental case, they are respectively $S_{w,P,E}$=18 μm/% and $S_{w,h,E}$=0.67 μm/μm.

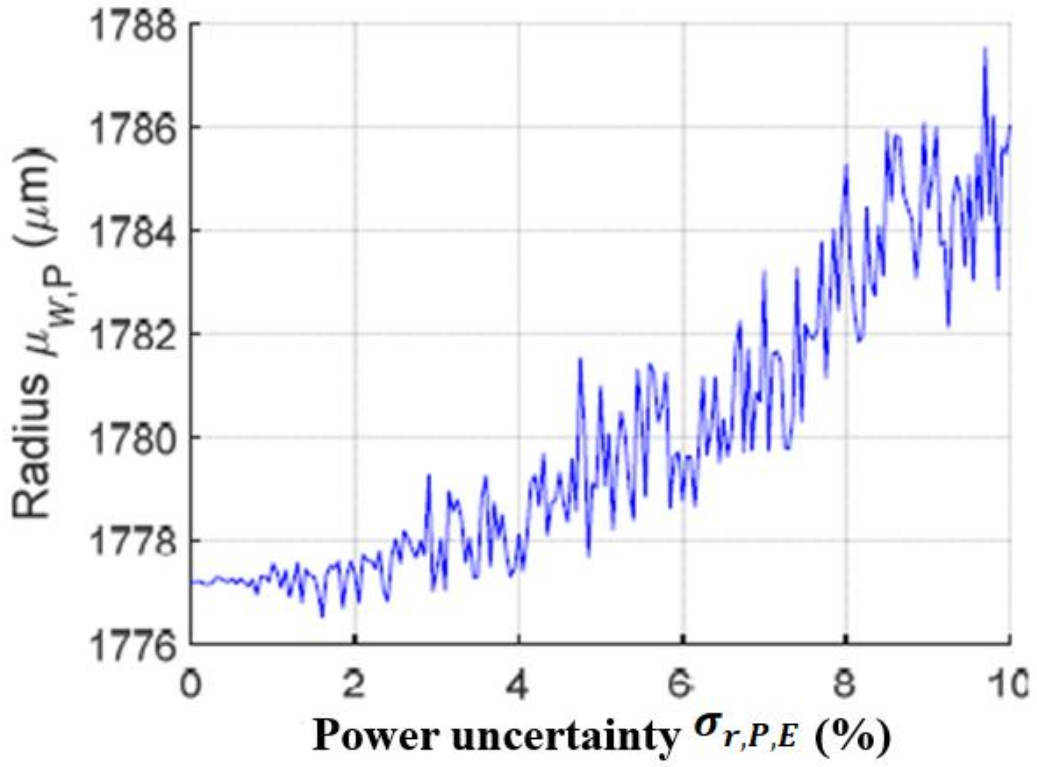

Figure 3.5 Erbium laser spot-size average value as a function of relative noise $\sigma_{r,P,E}$ on the erbium laser power

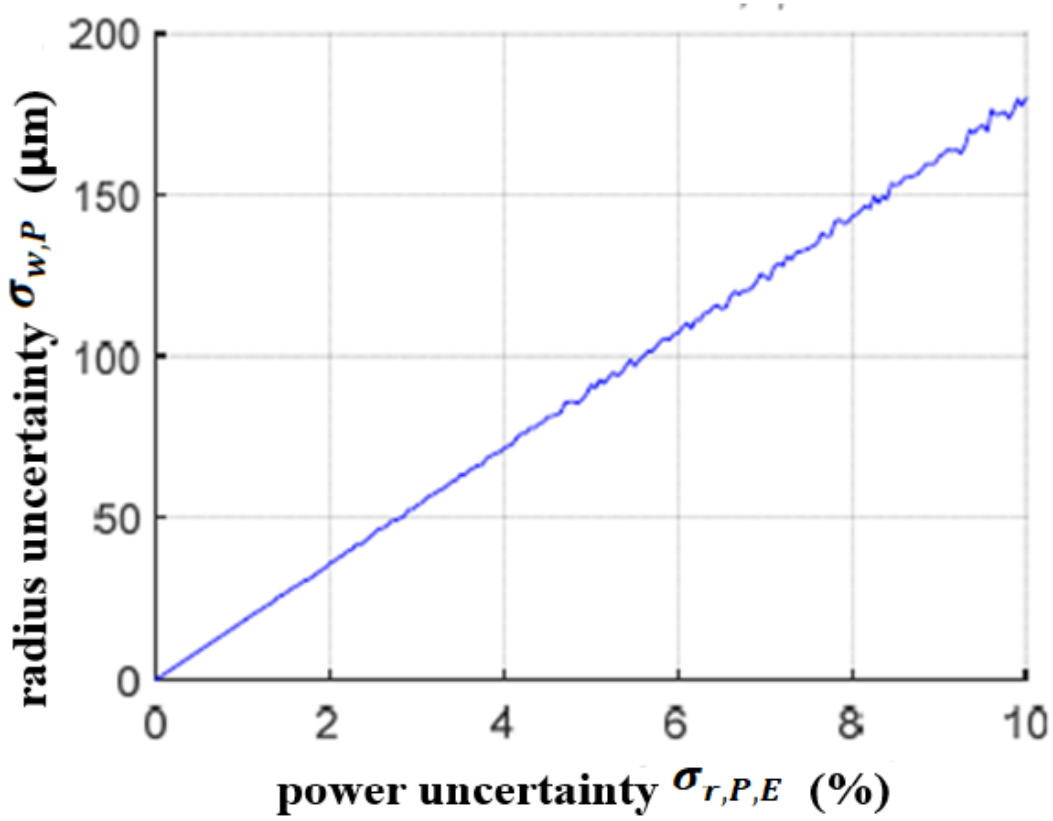

Figure 3.6 Erbium laser spot-size uncertainty as a function of relative noise $\sigma_{r,P,E}$ on the erbium laser power

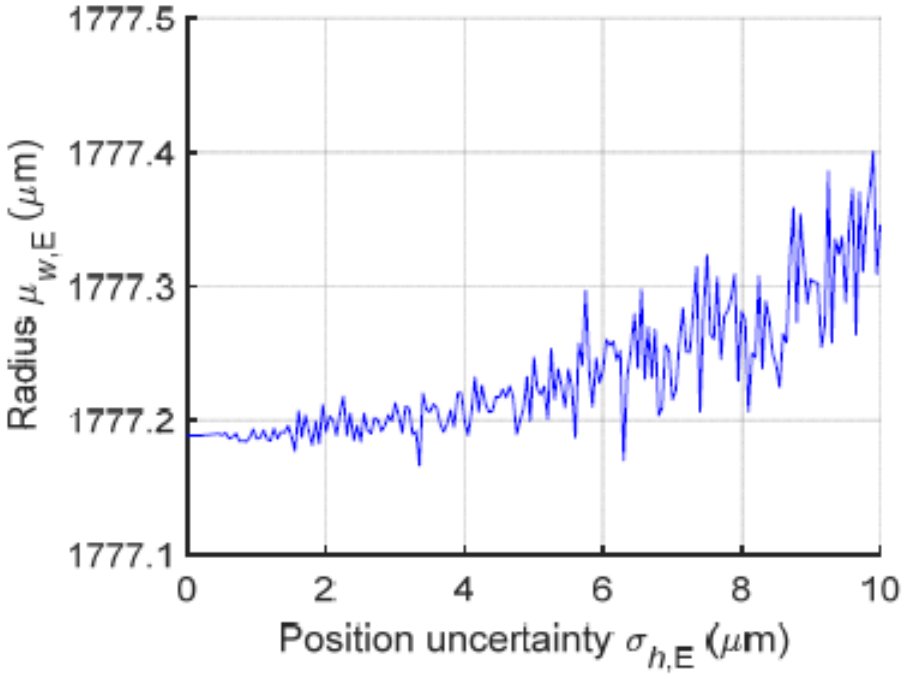

Figure 3.7 Erbium laser spot-size average value as a function of noise $\sigma_{h,E}$ on the K-E position

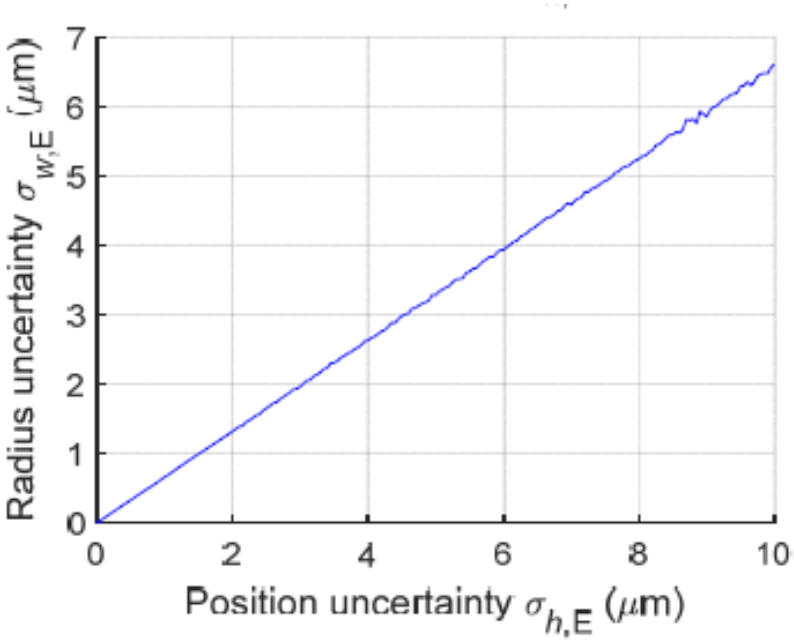

Figure 3.8 Erbium laser spot-size uncertainty as a function of noise $\sigma_{h,E}$ on the K-E position

The results 1_E and 2_E are similar to the ones of the pump laser. In the case of the erbium laser, bias errors in the measured beam radius w_E can reach a maximum of 8 μm for a laser-spot size of 1780 μm and relative noise on the laser optical power of 10%. Moreover, the result 3_E is useful when evaluating the combined standard uncertainty of the spot size *w*.

3.2 Comparative Analysis and Influential parameter

It has been proved that the sensitivities of the spot-size uncertainty depend on the specific experimental conditions when measured by the knife-edge technique. This has been demonstrated by the different sensitivities calculated in independent spot-size measurements with the knife-edge method on two different experiments, using laser beams with different beam widths as well as optical powers. In particular, from some preliminary calculations upon changing the span of the position axis ($\Delta h_{SPAN}=h_{MAX}-h_{MIN}$) relative to the beam spot size w, both sensitivities of u(w) to noise in the laser power, u(P), and to noise in the blade position, u(h), do change, also depending on the adopted experimental spatial resolution $\Delta h_{EXP}=h_{i+1}-h_i$. The detailed mathematical analysis of these aspects is beyond the scope of this study.

The uncertainty sensitivities depend specifically on the experimental conditions. Particularly, various sensitivities are affecting the input uncertainties of the laser optical power and the knife-edge position. Moreover, the values of those two sensitivities do depend basically on the width of the positions data range with respect to the laser beam standard width, spot size. Once the spot size uncertainty and the measured spot-size sensitivities are known, the measurement uncertainty can be calculated. In this case, the main input variables are two:

1) The laser optical power P, which can be obtained by the laser output and measured by the power meter

2) The knife-edge position h, which can be obtained and measured by the micrometer translator.

To estimate these input variables uncertainties, we have to know the statistical behavior of the two measurable quantities and the expected values of the standard deviation of their means. Rapid and simplified analyses have to be performed to find out justifiable practical values of $u(P)$ and $u(h)$. For the pump laser, we have to put into consideration power instability along with time and the power meter instability, which are evaluated as 2 % and 1% respectively. Consequently, it is necessary to compensate by estimating $u_r(P_P)\approx 2.2$ % that we can translate in a constant overall power uncertainty $u(P_P)\approx 0.9$ mW~1 mW (for an average power value of 40 mW).

On the other hand, it is necessary to compensate for the observed erbium laser temporal instability, in the order of 5 % during the measurement times. Considering the power meter uncertainty of 1 % can be estimated as $u_r(P_E)\approx 5.1$ % that can be translated in a constant overall power uncertainty $u(P_E)\approx 1.3$ mW (for an average power value of 25 mW). As mentioned earlier, a micrometer is used to adjust the Knife Edge displacements and its resolution is $\Delta h=10$ μm. However, it is necessary to assume uncertainty in position in the order of $u(h_P)=u(h_E)\approx 2$ μm for both measurements, on pump laser and erbium laser. Substituting for these values in equation 3.1, we get the resulting uncertainty budgets and spot-size uncertainty values as shown in Table 3.1.

	$S_{w,P}$ (μm/%)	$S_{w,h}$ (μm/μm)	$u_r(P)$ (%)	$u(h)$ (μm)	$u(w)$ (μm)	$u_r(w)$ (%)	w (μm)
Pump laser (spot size w_P)	4.2	0.74	2.2	2	9.4	2.3%	405.6
Erbium laser (spot size w_E)	18	0.67	5.1	2	91.8	5.2%	1777

Table 3.1

Which indicates that for this kind of experiments, the two main uncertainties affecting the spot size uncertainty u(w) are:

- The power uncertainties, in the order of a few milliwatts (mW)

- The blade position uncertainty of a few micrometers (μm)

The uncertainty is influenced mainly by the power uncertainty, which has a higher impact. This is for the significantly higher sensitivity coefficient $S_{w,P}$ (μm/mW) with respect to $S_{w,h}$ (μm/μm) when expressed in these units. Based on this result, greater uncertainty improvement is expected when working on reducing the laser amplitude noise and power meter inaccuracy, instead of working on the much less useful reduction in the Knife Edge position uncertainty, Particularly, when the two sensitivity values are calculated using the method proposed to obtain the values as the ones given in points 3_P and 3_E for our lasers. Any other more detailed and comprehensive analysis to evaluate u(P) and u(h) can be carried out so that their estimated values can be inserted into equation 3.1, including the sensitivity values and input variables uncertainties, to get the laser spot-size measurement uncertainty which is greatly dominated by the laser power measurement uncertainty.

3.3 Reducing Uncertainty for the laser beam size measurements using a scanning edge approach

A slight modification in the process of analyzing the measurement of the Gaussian laser beam spot size method has been developed. The novel analysis greatly reduces the uncertainty in the estimation of the beam-spot size. Using the beam scanning approach in the measurement and fitting the data to an analytical approximation to the complementary error function, the obtained fitted parameters were consistent with the standard differentiation approach but with much smaller uncertainty. For a Gaussian laser beam, the intensity peaks at the center of the beam and it is described by

$$I(x,y) = I_0 \exp\left[-\frac{2(x-x_0)^2}{w_x^2} - \frac{2(y-y_0)^2}{w_y^2}\right] \qquad 3.2$$

, Where we have that w_x and w_y as the $1/e^2$ half widths in x and y directions and x_0 and y_0 as the values of x and y at the center of the beam. The maximum incident optical power on the power meter is $I_0 = 2P / \pi w_x w_y$, assuming a perfectly rounded laser. The knife-edge technique is based on scanning the laser beam with a blade attached to a micrometer while measuring the power incident on the power meter and plotting the measured power based on the position of the blade. For such a structure, the laser power incident on the power meter is governed by

$$s(x) = \int_x^\infty \int_{-\infty}^\infty I(x', y')dy'dx' \qquad 3.3$$
$$= I_0 w_y \sqrt{\frac{\pi}{2}} \int_x^\infty \exp[-2\,\frac{(x'-x_0)^2}{w_x^2}]dx'$$
$$= \frac{I_0 \pi w_x w_y}{2} \operatorname{erfc}[\frac{2(x-x_0)}{w_x}]$$
$$= P \operatorname{erfc}\,[\frac{2(x-x_0)}{w_x}]$$

The integral on the right of the second line is a complementary error function defined as

$$erfc(x) = \frac{1}{\sqrt{2\pi}} \int_x^\infty \exp(-\frac{u^2}{2})\,du \qquad 3.4$$

, and it is related to the error function as

$$\operatorname{erf}(x) = 1 - 2\,erfc\left(\sqrt{2}\,x\right) \qquad 3.5$$

It is not possible to integrate equation 3.4 analytically. However, it is possible to extract w_x from *s(x)* by numerically differentiating the measured value of *s* to the blade position *x*, where *s* has a Gaussian dependence on *x*. Then the one-dimensional Gaussian function of equation 3.2 is fitted to the derivative of *s* to give the desired w_x.

Now for Gaussian noise R(x) added to the ideal *s(x)* due to the measurement process, it is possible to express the probability distribution of *R*(*x*) as

$$P(R) = \frac{1}{\sigma\sqrt{2\pi}} \exp(-\frac{R^2}{2\sigma^2}) \qquad 3.6$$

Where σ represents the standard deviation of *R* from its mean value. If the mean is zero, the measured signal will then be

$$S(x) = s(x) + R(x) \qquad 3.7$$

By differentiating equation 3.7, we will obtain

$$\frac{dS(x)}{dx} = \frac{ds(x)}{dx} + \frac{dR(x)}{dx} = g(x) + D(x) \qquad 3.8$$

where *g*(*x*) is the one-dimensional Gaussian function resulted by differentiating s(*x*) while *D*(*x*) is the derivative of *R*(*x*). The probability distribution of *D*(*x*) can be calculated by the following argument. By subdividing *x* into discrete values x_i spaced by $\boldsymbol{\epsilon}$ and denoting the corresponding $R(x_i)$ by R_i and using the equation 3.6, the probability Pr of having the values of R_i and R_{i+1} such that $R \leq R_i \leq R +$ d*R* and $R' \leq R_{i+1} \leq R' +$ d*R* can be written as

$$\Pr[R' \leq R_i + 1 \leq R' + \mathrm{d}R,\ R \leq R_i \leq R + \mathrm{d}R\ ]$$
$$= P(R')dRP(R)dR$$
$$= \frac{1}{2\pi\sigma^2} \exp\left(-\frac{R^2+R'^2}{2\sigma^2}\right) dR^2 \qquad 3.9$$

This is equivalent to the probability of $R \leq R_i \leq R + \mathrm{d}R$ and $D \leq D_i \leq D + \mathrm{d}D$. In this case $D = R' - \frac{R}{\epsilon}$. consequently, Equation 3.9 guides us to

$$\begin{aligned} &\Pr[D \leq D_i \leq D + \mathrm{d}D, R \leq R_i \leq R + \mathrm{d}R] \\ &= \frac{\epsilon}{2\pi\sigma^2} \exp\left(-\frac{R^2+(D\epsilon)^2}{2\sigma^2}\right) dRdD \end{aligned} \qquad 3.9$$

And by integrating over R, the probability $D \leq D_i \leq D$ becomes

$$\begin{aligned} &\Pr[D \leq D_i \leq D] = P(D)dD \\ &= \int_{-\infty}^{\infty} \frac{\epsilon}{2\pi\sigma^2} \exp\left[-\frac{R^2+(D\epsilon)^2}{2\sigma^2}\right] dRdD \\ &= \frac{1}{\sigma'\sqrt{2\pi}} \exp(-\frac{D^2}{2\sigma'^2})\, dD \end{aligned} \qquad 3.10$$

given that $\sigma' = \sqrt{2}\sigma/\epsilon$. It is now obvious that the probability distribution of $D(x)$ is also Gaussian yet the width becomes larger as $\boldsymbol{\epsilon}$ is decreased. This is a result of the well-known fact that high-frequency noise in data gives elevates the scatter in the derivative of the data. Generally, while fitting a function to measured data, the greater the number of data points, the greater the confidence in the fit. However, for the conventional spot size measurements with a constant noise level, more data points yield less spacing in the independent variable *x* and thus an increase in σ', which is the effective scatter in the derivative of the data. Typically, one can try to neutralize this problem by applying a smoothing algorithm to the original data or the derivative of the data. However, there will be the side effect of broadening the curve of the profile, which is the width that we want to measure. For instance, figure 3.9- a and b show the data obtained by typical beam profile measurements using the scanning knife-edge technique. In figure 3.9 a there are 51 data points of the beam spot size measurements while figure 3.9 b contains only 26 data points. The corresponding numerical derivatives of these two data curves are demonstrated in figures 3.9-c and d respectively. There is an evident increase in the derivative noise.

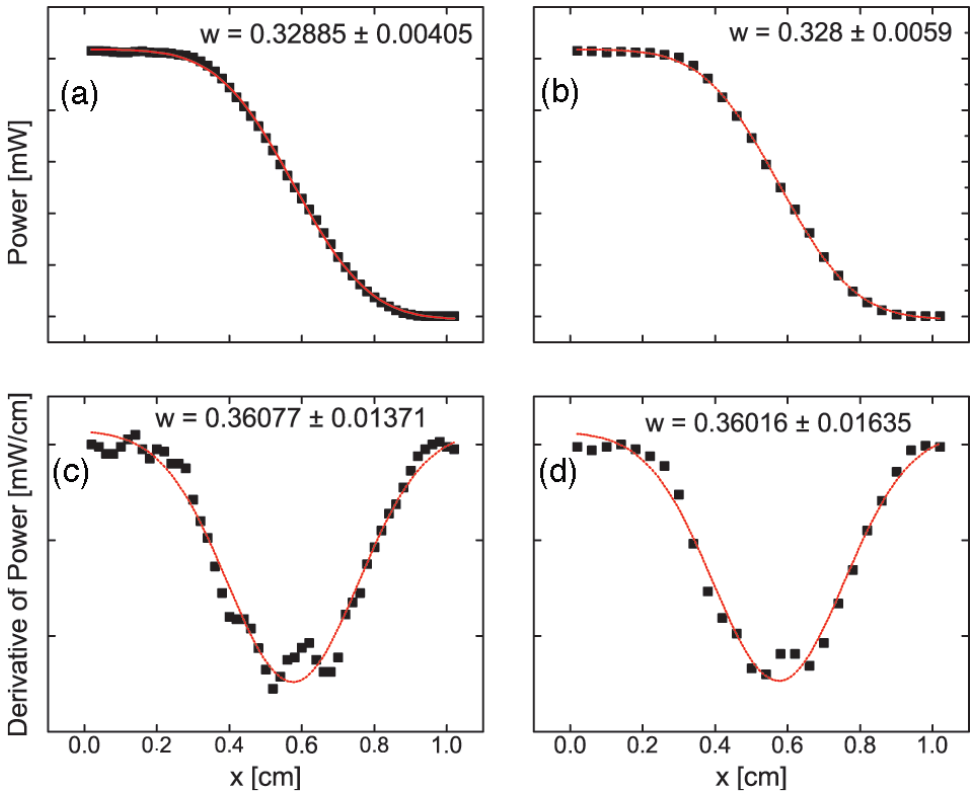

Figure 3.9 Points in (a) and (b) are the measurement of the laser beam spot size by the knife-edge technique. The dashed curves are fits to the complementary error function. The points in(c) and (d) are the derivatives of the data in (a) and (b), respectively. The dashed curves are fits to the Gaussians. (a) and (c) are for data containing 51 points, and (b) and (d) are for data containing 26points over the same range.

The proposed solution to fix the problem here is to not derive the data and instead fit them directly to the complementary error function in equation 3.3 and 3.5 when combined together to give

$$s(x) = \frac{P}{2}\left\{1 - \operatorname{erf}\left[\frac{\sqrt{2}(x - x_0)}{w_x}\right]\right\} \qquad 3.11$$

Where x is the position of the knife-edge, x_0 is the center of the beam, P is the total optical power contained in the beam, and w_x is the desired $1/e^2$ half-width. As mentioned earlier, the error functions cannot be integrated analytically yet there exist several approximations to the error function and are effectively accurate for the fit required. As an example the researchers used

$$\operatorname{erf}(x) = 1 - (a_1 t + a_2 t^2 + a_3 t^3)\exp(-x^2) + \epsilon(x)\ , \qquad 3.12$$

Where we have that $t = (1 + px)^{-1}$,

$p = 0.47047$,

$a_1 = 0.3480242$,

$a_2 = -0.0958798$,

$a_3 = -0.7478556$,

$|\boldsymbol{\epsilon}=(x)\leq 2.5 * 10^{-5}|$

The dashed lines in figures 3.9-a and 3.9-b represent the best fits of complementary error functions, using equations 3.11 and 3.12 to the data. The fitted parameters are the total power, Gaussian centers,

and widths. The values for the fitted widths, including the fitting uncertainties, are indicated in figure 3.9. The dashed curves in 3.9-c and 3.9-d are the fits of Gaussians in equation 2.1 to the derivatives of the data. The values for the fitted widths along with their uncertainties are indicated in the graphs. No pre-smoothing of the data was carried out. We note that while the widths for both fitting techniques came out virtually identical, the estimates of uncertainty in these widths are an order of magnitude greater for the conventional Gaussian fits than for the error function fits, due to the derivative induced scatter in the latter cases. To further demonstrate the advantage of fitting a complementary error function to the raw data rather than fitting a smoothed Gaussian to the derivative of the data, values of a complementary error function were generated by numerical integration of the Gaussian of equation 3.3 with width $w = 2$, to which the noise of Gaussian distribution had been added. This was done for two sets of data having the same interval in x, but having different numbers of points over that interval. Derivatives were computed for both sets of data. Table 3.2, summarizing the results of fitting the two types of functions to the corresponding data, shows good agreement with the expected behavior of fitting errors.

Number of Points	w_{erfc}	$w_{\text{derivative}}$
50	1.97 ± 0.02	1.8 ± 0.11
100	2.01 ± 0.01	2.03 ± 0.13

Table 3.2 summary of the results

3.4 Conclusion

Through this study, the importance of Lasers has been highlighted and its parameters of quality have been explained as well as the methods used to measure them. Among these methods, the simplest and the most effective one is the scanning Knife-Edge, which has been explained in details through this study. During the experiments, the numerical nonlinear fitting of experimental data was introduced in order to aid the calculations of uncertainty sensitivities. In order to evaluate the different sensitivities of the estimated beam radius uncertainty to the dominant uncertainty sources in the typical experimental conditions, it is possible to using estimated values for the uncertainties of the variables of the experiment (optical power and beam cutting position) and weighting them by their corresponding calculated sensitivities. Then it is possible to retrieve the combined uncertainty of the indirect measurement of laser beam spot-size. By the method introduced in the paper, it is possible to calculate the two sensitivities ($S_{w,P}$ and $S_{w,h}$) of the measured beam radius uncertainty, $u(w)$, to the optical power relative uncertainty, $u_r(P)$, and to the Knife-Edge position uncertainty, $u(h)$. Starting from the experimental data, it is possible to find sensitivities as the ones obtained in points 3_P and 3_E for the case of these specific types of lasers and their measured beam radii. Calculated sensitivities can be inserted into equation 3.1 with the estimates of the input uncertainties (optical power and the knife-edge positions), to get the measurement uncertainty of the laser Gaussian beam radius. These two sensitivities depend on the experimental conditions and most importantly they change with the specific width of the knife-edge positions data range and with the knife-edge position steps for a specific laser beam radius. These behaviours of uncertainty sensitivities can addressed in a future work. It has also been clarified during the process of analysing the data obtained by the Knife-Edge technique that it is more advantageous to directly fit the data to a numerical approximation of the

complementary error function instead of fitting the derivative of the data to a Gaussian. The main advantage is that by taking the derivative, scatter is introduced in the data and this will decrease the confidence in fitted width. Despite that it was is demonstrated in this work, smoothing operations to the data, either before or after taking the derivative, runs the risk of artificially increasing the apparent spot width.

References

R. L. McCally, “Measurement of Gaussian beam parameters,” July 1984.

K. D. Kirkham and C. B. Roundy, “Current Technology of Beam Profile Measurement,” in Fred M. Dickey, *Laser Beam Shaping: Theory and Techniques*, 2nd Ed., Boca Raton, FL, USA: CRC Press, 2017. ISBN 9781138076303

J. A. Arnaud, W. M. Hubbard, G. D. Mandeville, B. de la Clavière, E. A. Franke, and J. M. Franke, “Technique for Fast Measurement of Gaussian Laser Beam Parameters,” 1971.

J. M. Khosrofian and B. A. Garetz, “Measurement of a Gaussian laser beam diameter through the direct inversion of knife-edge data,” *Appl. Opt*. Nov. 1983.

G. Veshapidze, M. L. Trachy, M. H. Shah, and B. D. De Paola, “Reducing the uncertainty in laser beam size measurement with a scanning edge method,” *Appl. Opt*. Nov. 2006.

M. González-Cardel, P. Arguijo, and R. Díaz-Uribe1, “Gaussian beam radius measurement with a knife-edge: a polynomial approximation to the inverse error function,” June 2013.

Pedro da Silva Hack and Carla Schwengber ten Caten, “Measurement Uncertainty: Literature Review and Research Trends,” *IEEE Trans. Instrum. Meas*. 8, Aug. 2012.

Y. Suzaki and A. Tachibana, “Measurement of the μm sized radius of Gaussian laser beam using the scanning knife-edge,” Dec. 1975.

M. Abramowitz and I. A. Stegun, eds., *Handbook of Mathematical Functions* (National Bureau of Standards, 1964).

N. G. Kingsbury, “Lecture notes on ‘digital modulation,’” Courses I5 and 3F4, Department of Engineering, University of Cambridge, 1995–2005.